Electronic Supplementary Material (ESI) for Journal of Materials Chemistry A.
This journal is © The Royal Society of Chemistry 2020

# Electronic Supplementary Information

## Two-Dimensional Covalent-Organic Frameworks for Ultrahigh Iodine Capture

Jinheng Li[a], Huixin Zhang[a], Lingyan Zhang[a], Ke Wang[a], Zhengkang Wang[a], Guiyan Liu[a,*], Yanli Zhao[b,*], Yongfei Zeng[a,c*]

[a] *Tianjin Key Laboratory of Structure and Performance for Functional Molecules, Key Laboratory of Inorganic–Organic Hybrid Functional Material Chemistry (Ministry of Education), College of Chemistry, Tianjin Normal University, Tianjin, 300387, P. R. China. E-mail: guiyanliu2013@163.com (Guiyan Liu); yfzeng@nankai.edu.cn (Yongfei Zeng).*

[b] *Division of Chemistry and Biological Chemistry, School of Physical and Mathematical Sciences, Nanyang Technological University, 21 Nanyang Link, 637371 Singapore. Email: zhaoyanli@ntu.edu.sg (Yanli Zhao).*

[c] *Key Laboratory of Advanced Energy Materials Chemistry (Ministry of Education), College of Chemistry, Nankai University, Tianjin 300071, China*

**Table of Contents**


| | Section | Page |
|---|---|---|
| S1 | General Information and Materials | S2 |
| S2 | Synthetic Procedures | S3 |
| S3 | Fourier Transform Infrared Spectroscopy | S7 |
| S4 | Nuclear Magnetic Resonance Spectroscopy | S8 |
| S5 | Scanning Electron Microscope | S10 |
| S6 | Thermogravimetric Analysis | S11 |
| S7 | Powder X-ray Diffraction | S12 |
| S8 | Structural Modeling and Crystallographic Data | S13 |
| S9 | Porosity and Specific Surface Area Analysis | S27 |
| S10 | Iodine Vapor Uptake and Release Experiments | S30 |
| S11 | References | S41 |

## S1. General Information and Materials

### Materials

Tris(4-formylphenyl)amine was purchased from Shanghai Tensus Biotech Co., Ltd (Shanghai, China). 1,3,5-Tris(p-formylphenyl)benzene was purchased from Jilin Yanshen Technology Co., Ltd (Changchun, China). N,N-dimethylformamide (99.5%) and tetrahydrofuran (99.0%) were purchased from Tianjin JingDongTianZheng Precision Chemical Reagent Factory (Tianjin, China). Chlorobenzene (99%) and *o*-dichlorobenzene (99%) and were purchased from Sigma Aldrich Chemicals.

### Analytical techniques

Fourier transform infrared (FT-IR) spectra were recorded as KBr-pellet on a Nicolet IR200 FT-IR spectrometer. $^{1}$H NMR and $^{13}$C NMR spectra were recorded on a Bruker AV 400MHz spectrometer (Bruker). Solid-state $^{13}$C NMR spectra were recorded on a VARIAN Infinity plus 300 MHz. Thermogravimetric analysis (TGA) was carried out under nitrogen flow (60 mL/min) on a TGA Q500 thermoanalyzer with a heating rate of 15 °C /min. Powder X-ray diffraction (PXRD) data were collected at 40 kV, 40 mA on a Bruker D8 Advance diffractometer using Cu-Kα radiation over $2\theta$ range of 3°-30° at room temperature. Gas sorption analyses were conducted using Quantachrome Instruments Autosorb-iQ-MP-MP with extra-high pure $N_2$. The samples treated by THF were loaded into a sample cell and dried under vacuum at 60 °C and 150 °C by using the "outgasser" function for 1 h and 12 h before the measurements, respectively. The Brunauer−Emmett−Teller (BET) surface area and pore size distribution were calculated from the $N_2$ sorption isotherms at 77 K. BET surface area calculations were carried out using the software provided within Quantachrome. Isotherm points chosen to calculate the BET surface area were subjected to the three consistency criteria. First, the pressure range selected should have values of $v(P_0 - P)$ increasing with $P/P_0$. Second, the points used to calculate the BET surface area must be linear with an upward slope. Third, the line they form must have a positive y-intercept. The pore size distribution was calculated based on the Quenched-Solid Density Functional Theory (QSDFT equilibrium model on carbon containing slit/cylindrical pores) model in the Quantachrome ASiQwin 3.01 software package. The scanning electron microscopy images were obtained on a FEI Nova Nano 230 Field-Emission, operating at an acceleration voltage of 15 kV. Metal Au sputtering (2×90 s) of the samples was necessary. UV/visible (UV/vis) spectra of the iodine solution were recorded using a UV-2600 UV/vis spectrophotometer within the wavelength range 200-600 nm. The Raman spectra were recorded on a Thermo Fisher DXR equipped with a 532 nm laser.

## S2. Synthetic Procedures

### Synthesis of 1,3,5-trimethyl-2,4,6-tris(4-nitrophenyl)-benzene

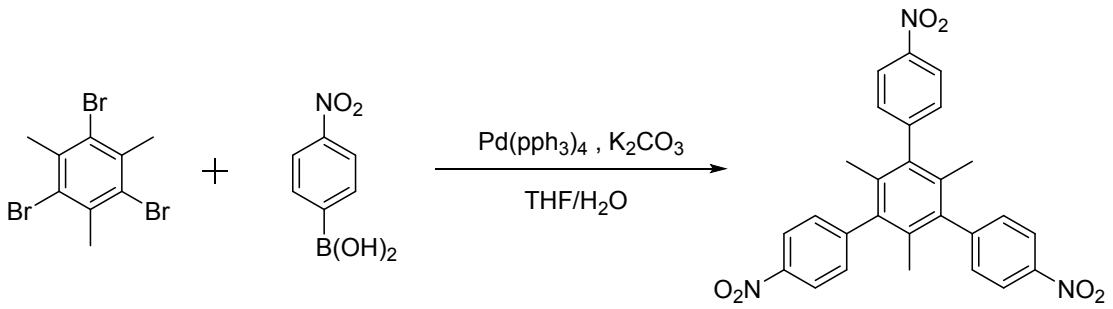


1,3,5-Trimethyl-2,4,6-tribromo-benzene (0.73 g, 10 mmol), 4-nitrophenylboronic acid (1.5 g, 45 mmol), tetrakis(triphenylphosphine)palladium (0.3 g, 1.3 mmol) and potassium carbonate (5.52 g, 200 mmol) were added to a flask. Then, tetrahydrofuran (THF)/water (2:1 v/v) solution (60 mL) was added to above mixture, followed by heating at 65 °C for about 30 hours. After the mixture was cooled to the room temperature, the THF was evaporated under reduced pressure. The residence was extracted with methylene chloride, and dried with anhydrous sodium sulfate. After evaporating the solvent, the crude product was obtained. After further purification using column chromatography (petroleum ether/dichloromethane = 5/1 v/v), a pure product was obtained as a white solid. $^{1}$H NMR (400 MHz, $CDCl_3$): δ (ppm) 8.34 (d, $J$ = 8 Hz, 6H), 7.41 (d, d, $J$ = 8 Hz, 6H), 1.68 (s, 9H); $^{13}$C NMR (101 MHz, $CDCl_3$): δ (ppm) 148.2, 147.1, 138.4, 132.9, 130.5, 124.1, 19.4.

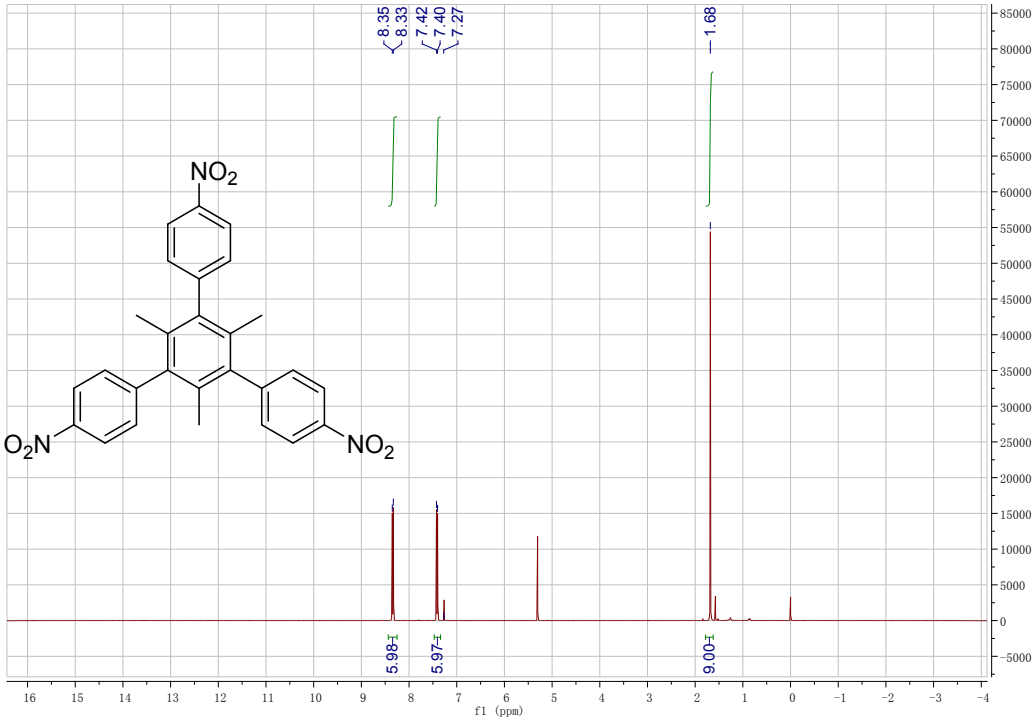


**Figure S1.** $^{1}$H NMR spectrum of 1,3,5-trimethyl-2,4,6-tris(4-nitrophenyl)-benzene.

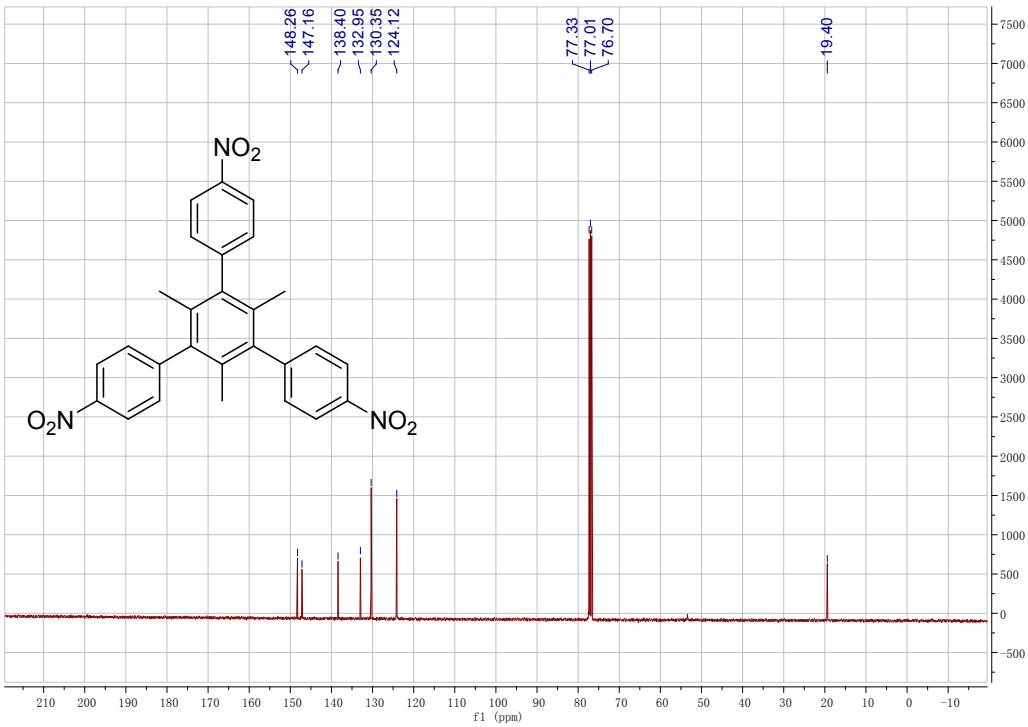


**Figure S2.** $^{13}$C NMR spectrum of 1,3,5-trimethyl-2,4,6-tris(4-nitrophenyl)-benzene.

**Synthesis of 1,3,5-trimethyl-2,4,6-tris(4-aminophenyl)-benzene**

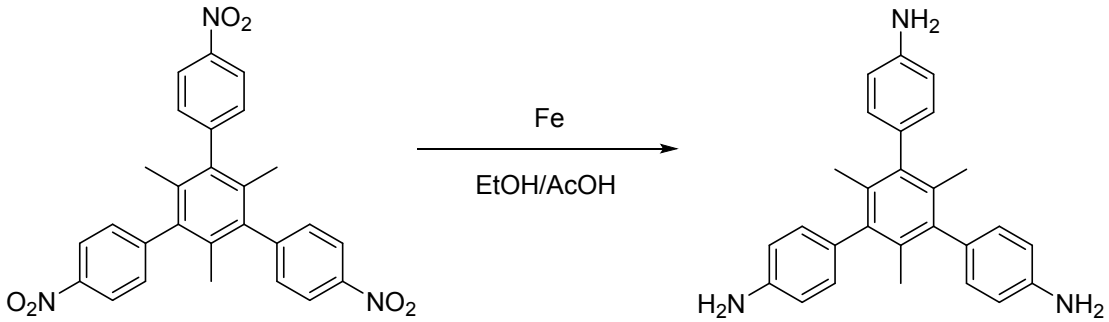


1,3,5-Trimethyl-2,4,6-tris(4-nitrophenyl)-benzene (0.664 g, 1.38 mmol) and iron (0.927 g, 16.56 mmol) were mixed in a flask. Then, a mixed solution of 1:1 v/v absolute ethanol/acetic acid (50 mL) was added into the above mixture, followed by refluxing at 80 °C for 3 hours. After the solution was cooled to the room temperature, the ethanol was evaporated under reduced pressure. The solution was extracted with methylene chloride, and dried over anhydrous sodium sulfate. After evaporating the solvent, the product was further purified using column chromatography (methylene chloride/ethyl acetate = 5/1 v/v), and a pure product was obtained as a white solid. $^{1}$H NMR (400 MHz, $CDCl_3$): δ (ppm) 6.99 (d, $J$ = 8 Hz, 6H), 6.74 (d, $J$ = 8 Hz, 6H), 3.65 (s, 6H), 1.76 (s, 9H); $^{13}$C NMR (101 MHz, $CDCl_3$): δ (ppm) 144.5, 139.6, 134.1, 132.7, 130.2, 115.2, 19.5.

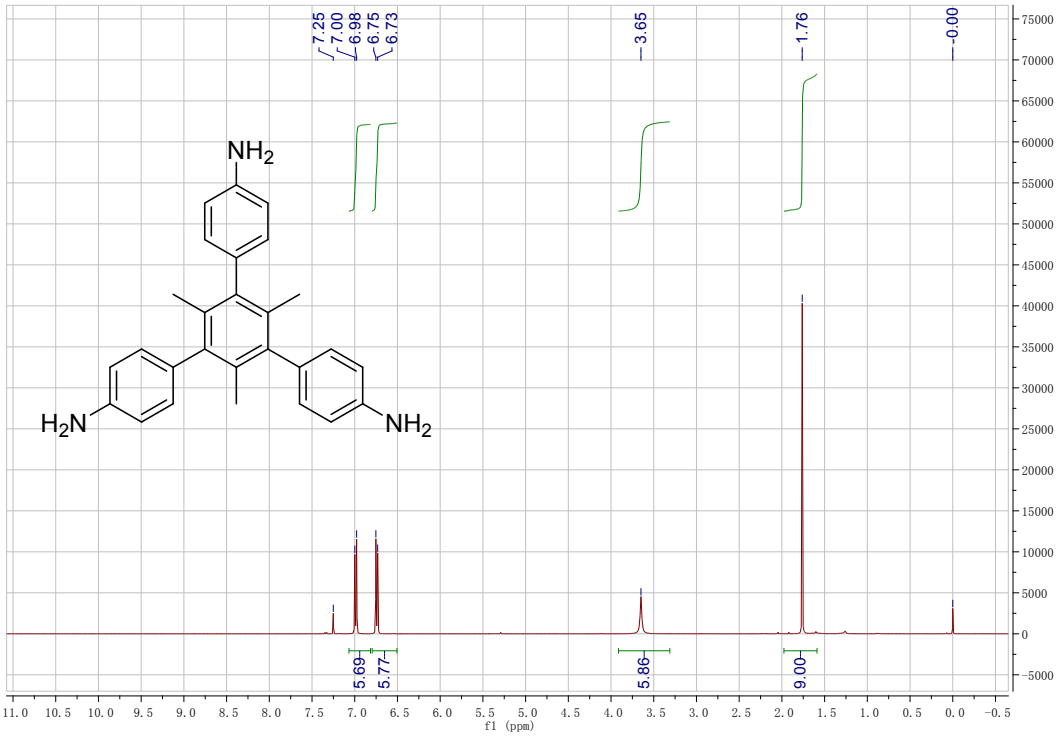


**Figure S3.** $^{1}$H NMR spectrum of 1,3,5-trimethyl-2,4,6-tris(4-aminophenyl)-benzene.

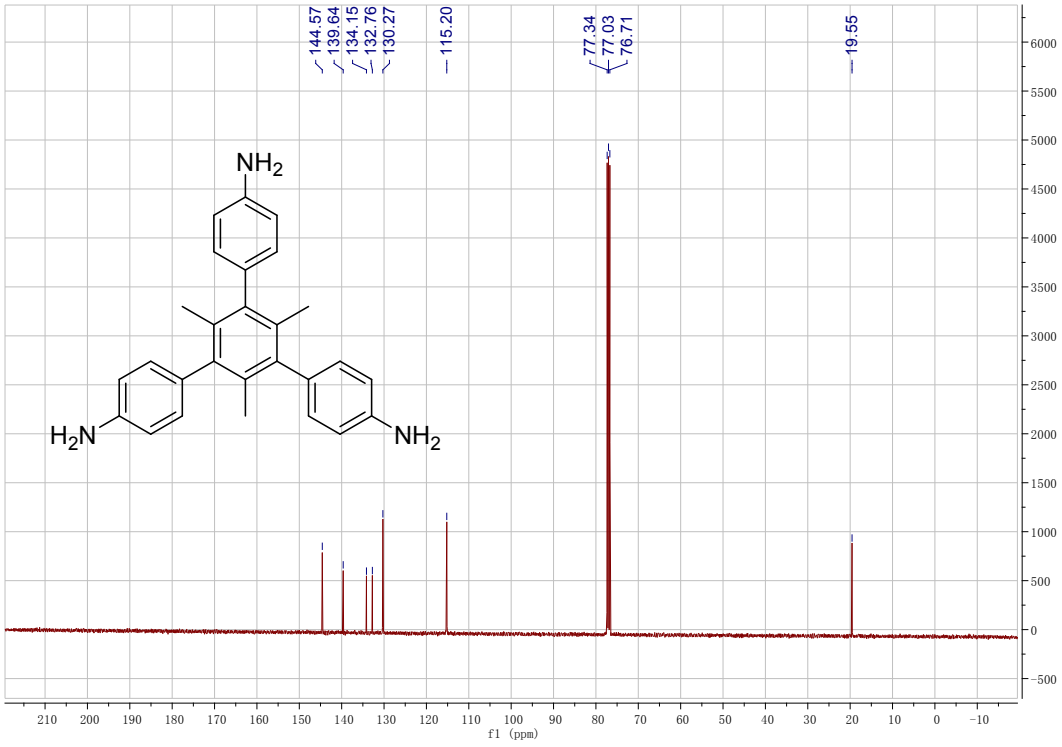


**Figure S4.** $^{13}$C NMR spectrum of 1,3,5-trimethyl-2,4,6-tris(4-aminophenyl)-benzene.

**Synthesis of TJNU-201:**

1,3,5-Trimethyl-2,4,6-tris(4-aminophenyl)-benzene (0.05 mmol, 19.6 mg) and tris(4-formylphenyl)amine (0.05 mmol, 16.46 mg) were added to a 10 mL Pyrex tube. Then, *o*-dichlorobenzene (2 mL) and 10 M acetic acid (0.2 mL) were added to the mixture. The freezing-vacuum-thaw cycle was performed three times under 77 K liquid nitrogen. The tube was sealed and heated at 120 °C for 3 days. After cooling to room temperature, the solid was filtered off and washed with DMF (3×5 mL) and THF (3×5 mL), respectively. After activated at 120 °C under vacuum for 12 h, the pure product, named TJNU-201, was obtained as a yellow powder.

**Synthesis of TJNU-202:**

1,3,5-Trimethyl-2,4,6-tris(4-aminophenyl)-benzene (0.05 mmol, 19.6 mg) and 1,3,5-tris(*p*-formylphenyl)benzene (0.05 mmol, 19.6 mg) were added to a 10 mL Pyrex tube. Then, chlorobenzene (2 mL) and 10 M acetic acid (0.2 mL) were added to the mixture. The freezing-vacuum-thaw cycle was performed three times under 77 K liquid nitrogen. The tube was heated at 120 °C for 3 days. After cooling to room temperature, the solid was filtered off and washed with DMF (3×5 mL) and THF (3×5 mL), respectively. After activated at 120 °C under vacuum for 12 h, the pure product, named TJNU-202, was obtained as an off-white powder.

## S3. Fourier Transform Infrared Spectroscopy

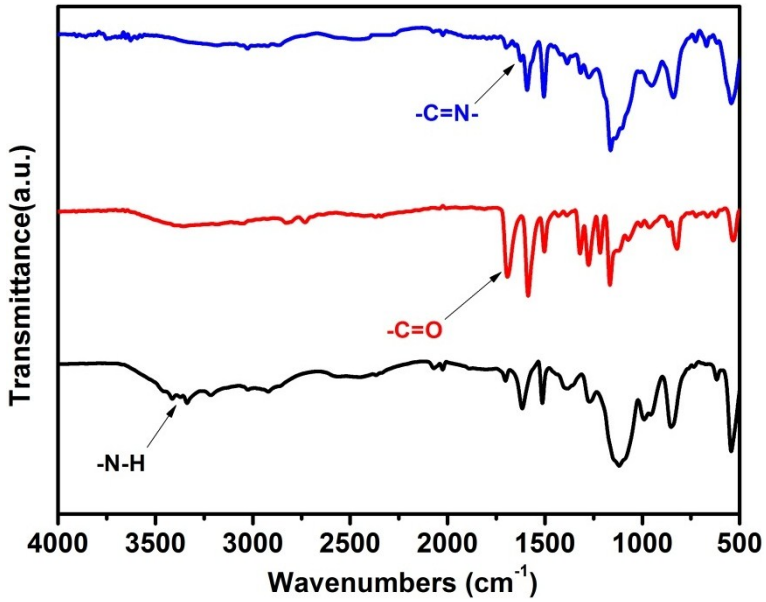


**Figure S5.** FT-IR spectra of 1,3,5-trimethyl-2,4,6-tris(4-aminophenyl)-benzene (black line), tris(4-formylphenyl)amine (red line), and TJNU-201 (blue line).

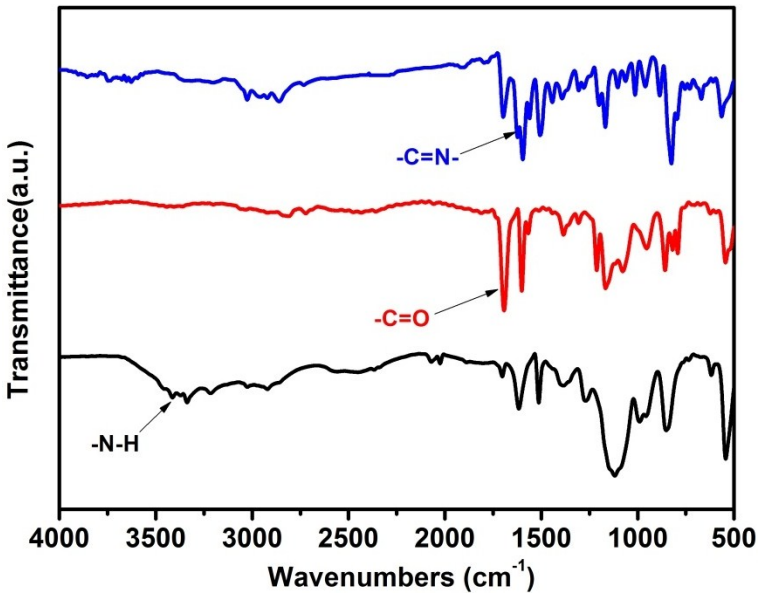


**Figure S6.** FT-IR spectra of 1,3,5-trimethyl-2,4,6-tris(4-aminophenyl)-benzene (black line), 1,3,5-tris(p-formylphenyl)benzene (red line), and TJNU-202 (blue line).

## S4. Nuclear Magnetic Resonance Spectroscopy

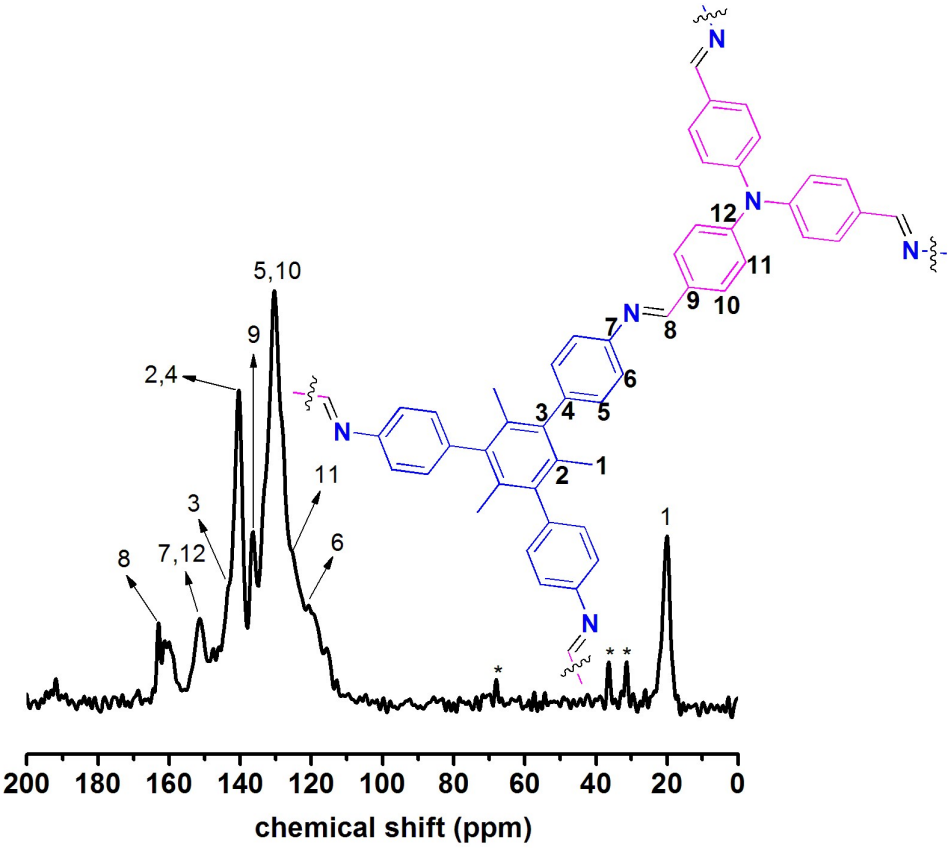


| Carbon number | Chemical shift (ppm) | Carbon number | Chemical shift (ppm) |
|---|---|---|---|
| 1 | 19 | 7 | 152 |
| 2 | 141 | 8 | 162 |
| 3 | 143 | 9 | 136 |
| 4 | 141 | 10 | 130 |
| 5 | 130 | 11 | 126 |
| 6 | 121 | 12 | 152 |

**Figure S7.** Solid-state $^{13}C$ NMR spectrum and peak assignments of TJNU-201. Asterisks denote spinning sidebands.

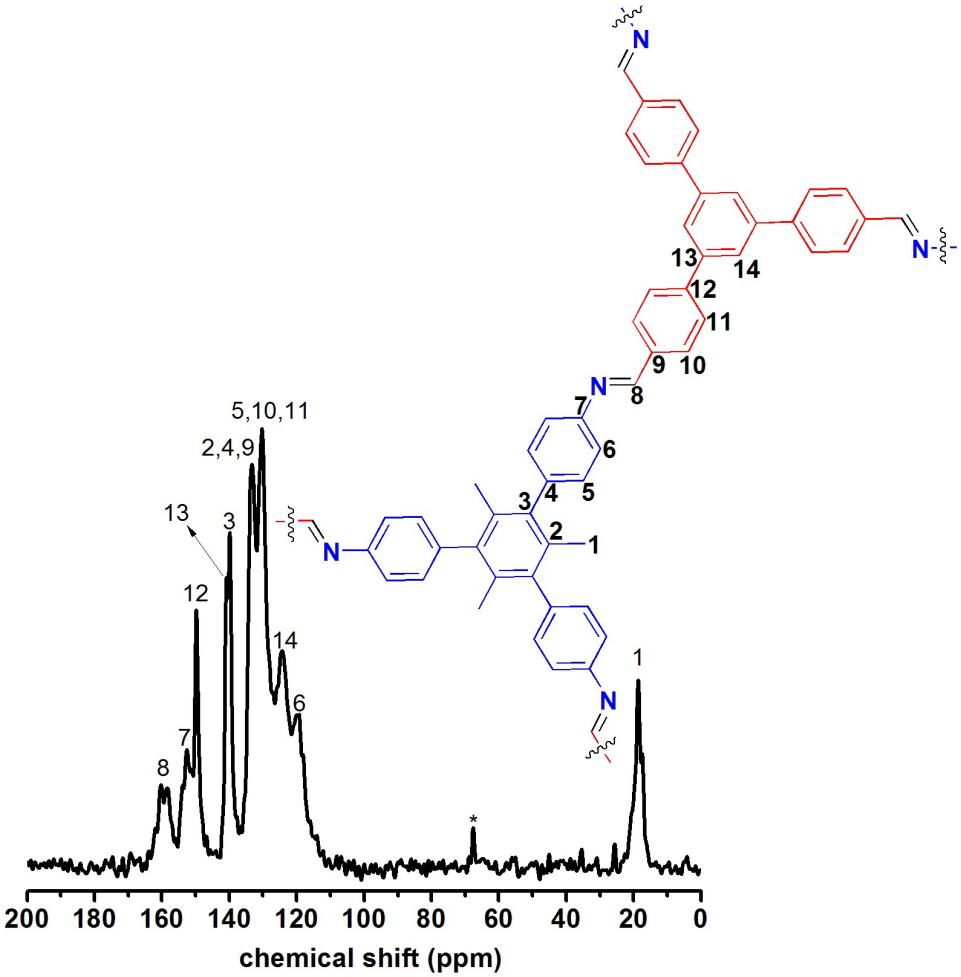


| Carbon number | Chemical shift (ppm) | Carbon number | Chemical shift (ppm) |
|---|---|---|---|
| 1 | 19 | 8 | 160 |
| 2 | 133 | 9 | 133 |
| 3 | 139 | 10 | 130 |
| 4 | 133 | 11 | 130 |
| 5 | 130 | 12 | 149 |
| 6 | 120 | 13 | 140 |
| 7 | 152 | 14 | 124 |

**Figure S8.** Solid-state $^{13}C$ NMR spectrum and peak assignments of TJNU-202. Asterisks denote spinning sidebands.

## S5. Scanning Electron Microscope

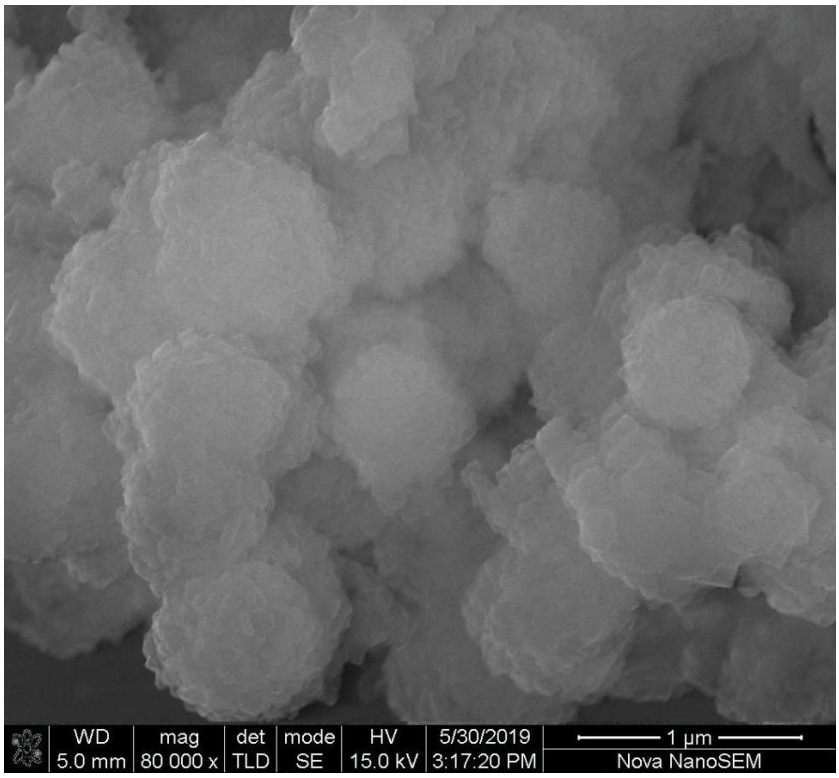


**Figure S9.** SEM image of TJNU-201.

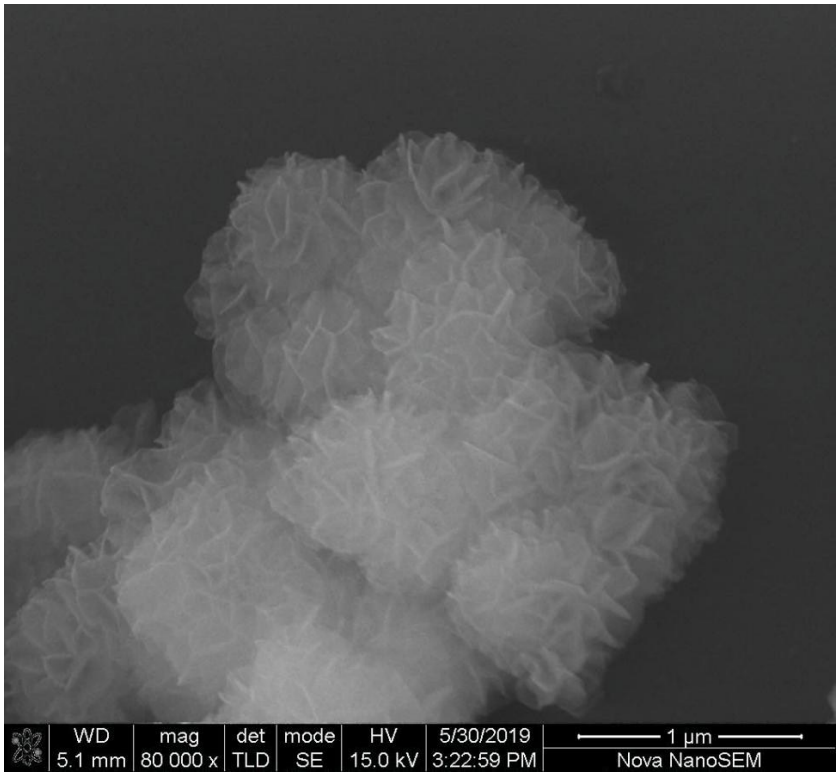


**Figure S10.** SEM image of TJNU-202.

## S6. Thermogravimetric Analysis

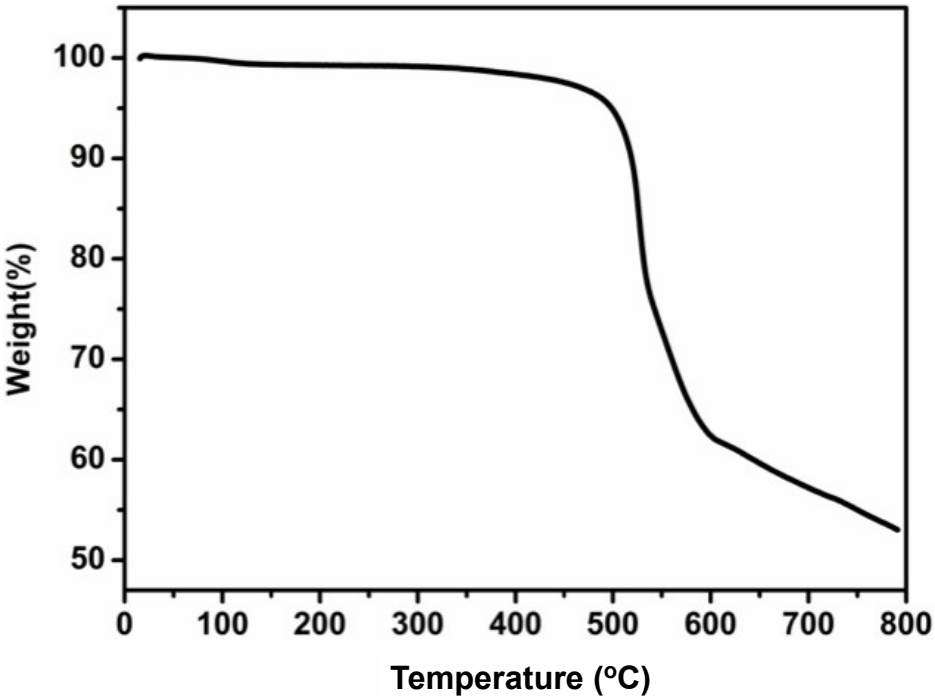


**Figure S11**. TGA curve of TJNU-201.

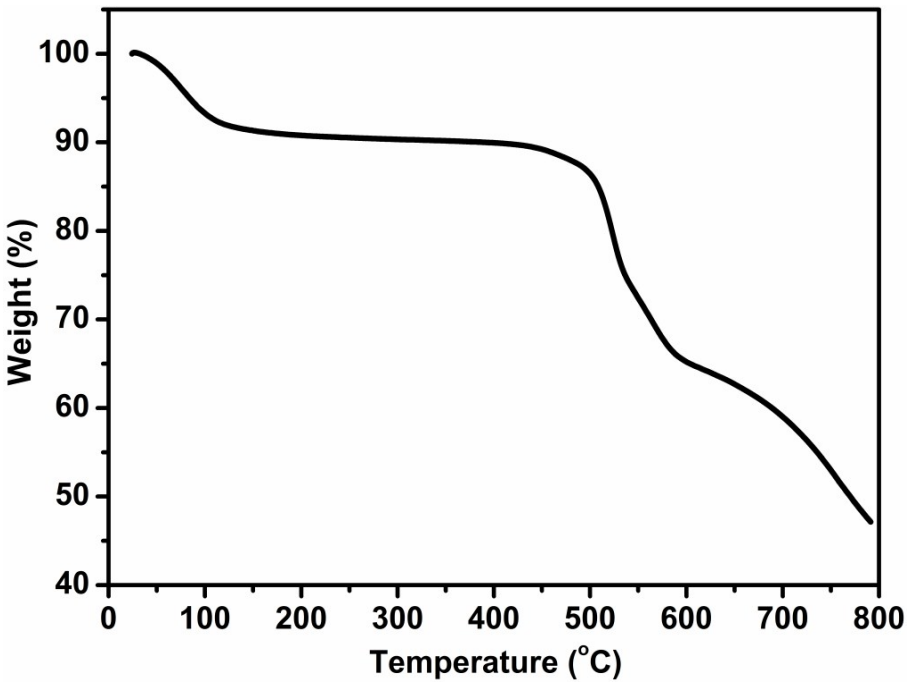


**Figure S12**. TGA curve of TJNU-202.

## S7. Powder X-ray Diffraction Analysis

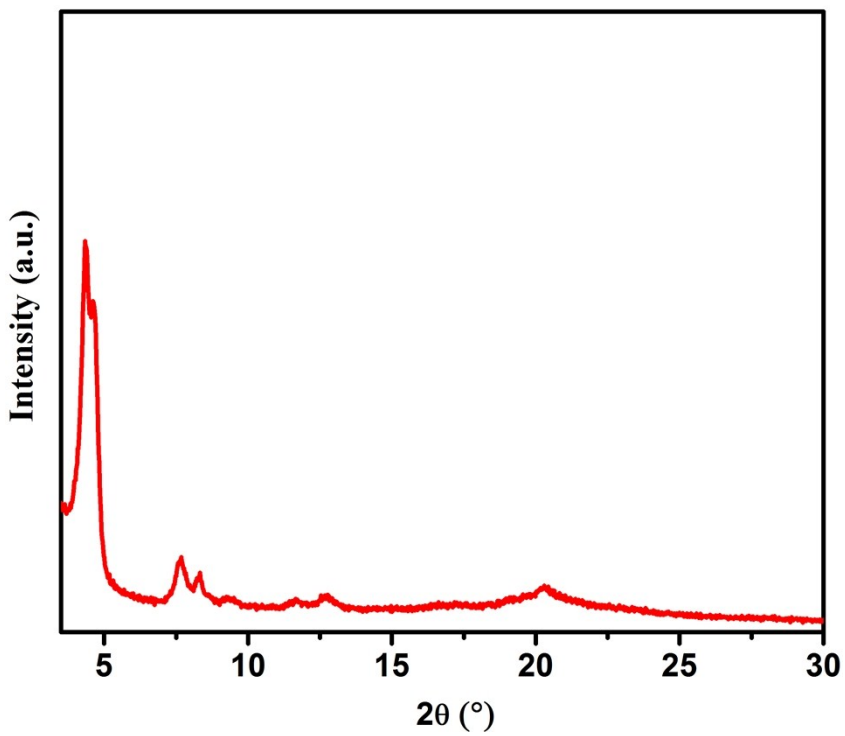


**Figure S13.** Experimental PXRD pattern of TJNU-201.

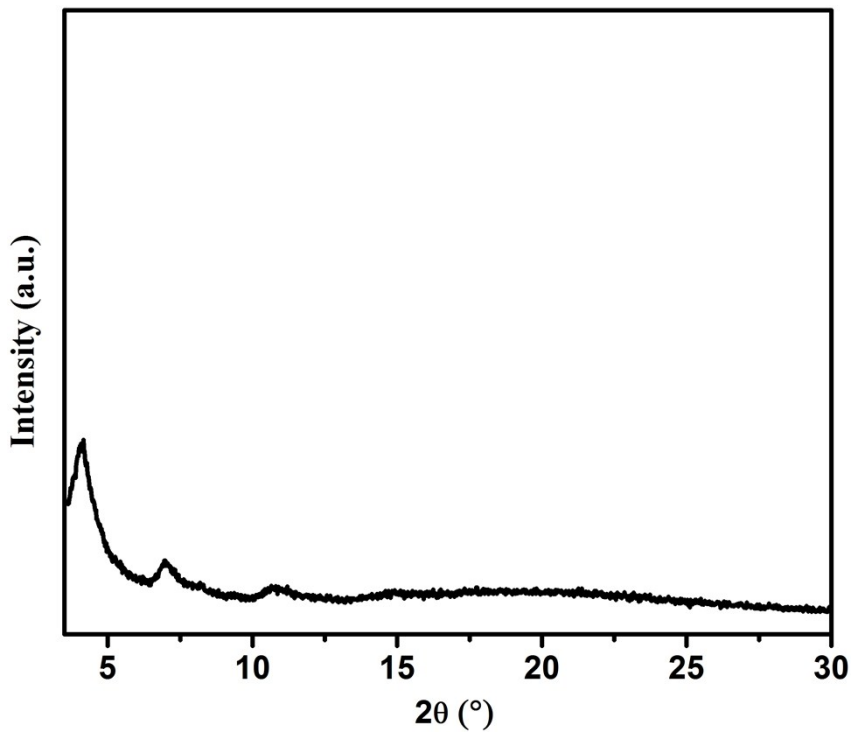


**Figure S14.** Experimental PXRD pattern of TJNU-202.

## S8. Structural Modeling and Crystallographic Data

The structure of TJNU-201 and TJNU-202 was determined by PXRD analysis, where the molecular modeling and Pawley refinement were carried out using Reflex, a software package implemented in MS modeling version, 4.4 (Accelrys Inc).[S1] Firstly, the lattice model was geometrically optimized using the MS Forcite molecular dynamics module. Then, we established the unit cell for TJNU-201 based on the space group of *P*3 (no. 143). Both the eclipsed and staggered stacking modes were considered for TJNU-201. For the staggered arrangement (Figure S15), the simulated PXRD patterns did not match with the experimental patterns. For the eclipsed structure (Figure S17), the simulated PXRD patterns did not perfectly match with the experimental patterns. Thus, 2D structure with a staircased stacking bnn net in the space group of *P*1 (no. 1), in which adjacent sheets were slipped by 2.0 Å along both *a* and *b* directions with much lower total energy, was modeled for TJNU-201. The unit cell parameters were $a$ = 23.655 Å, $b$ = 23.655 Å, $c$ = 4.800 Å, $\alpha$ = 78.00 °, $\beta$ = 78.00 ° and $\gamma$ = 120.00 ° for TJNU-201. The simulated PXRD pattern was in excellent agreement with the experimental one (Figure S18). Finally, Pawley refinement was performed to optimize the lattice parameters iteratively until the RWP value converged (Figure S19), yielding good agreement factors ($a$ = 23.654 Å, $b$ = 23.655 Å, $c$ = 4.800 Å, $\alpha$ = 78.15 °, $\beta$ = 78.04 °, $\gamma$ = 119.96 °, wRp = 0.94%, Rp = 0.66%). 3D structure of TJNU-201 with SrS topology based on $P2_13$ space group was also considered, and the simulated pattern did not match the experimental PXRD pattern (Figures S16).

For TJNU-202, the unit cell was constructed based on the space group of *P*3 (no. 143). Both the eclipsed and staggered stacking modes were considered for TJNU-202. For the staggered arrangement (Figure S21), the simulated PXRD patterns did not match with the experimental patterns. For the eclipsed structure (Figure S23), the simulated PXRD patterns matched well with the experimental patterns. The unit cell parameters were $a$ = 25.022 Å and $c$ = 4.150 Å for TJNU-202. Finally, Pawley refinement was performed to optimize the lattice parameters iteratively until the RWP value converged (Figure S24), yielding good agreement factors ($a$ = 25.023 Å and $c$ = 4.153 Å, wRp = 3.93%, Rp = 3.07%). 3D structure of TJNU-202 with SrS topology based on $P2_13$ space group was also considered, and the simulated pattern did not match the experimental PXRD pattern (Figures S22).

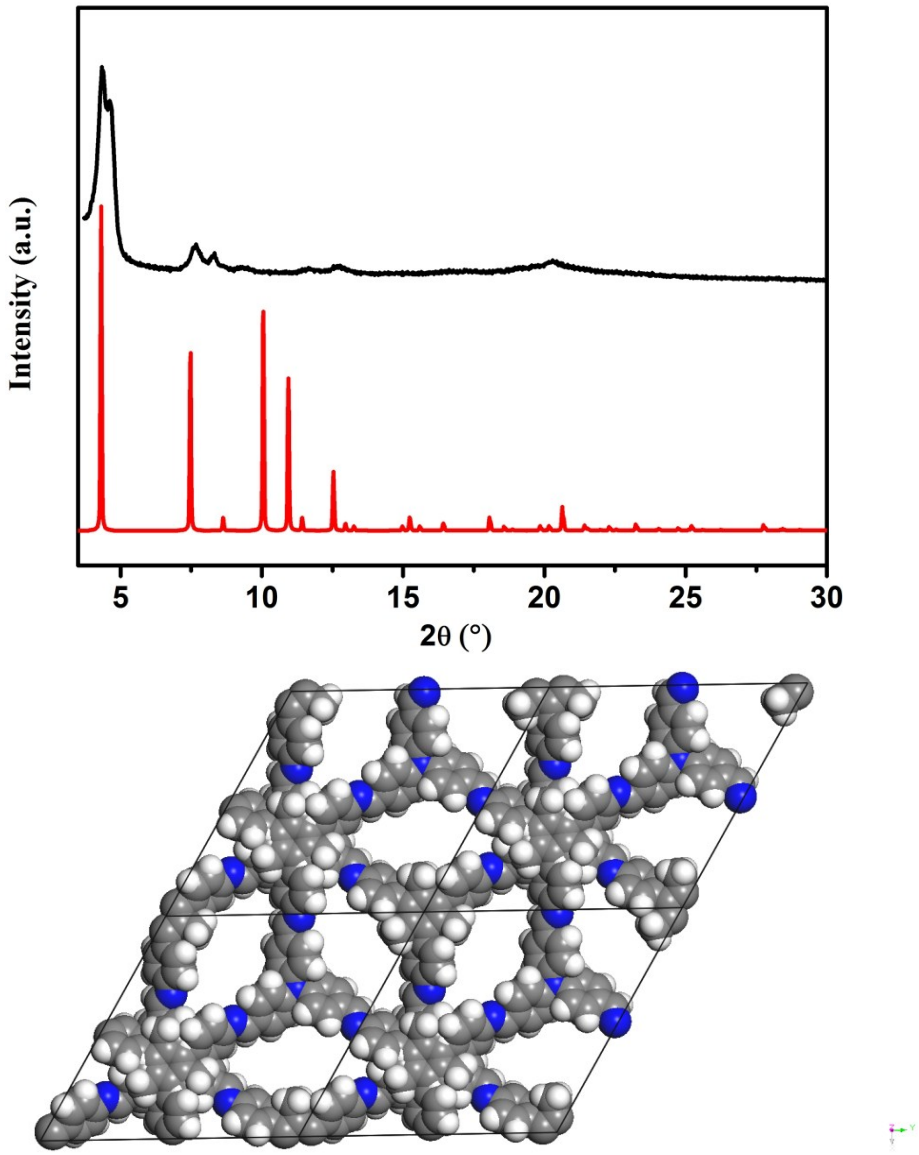


**Figure S15.** (Top) Experimental PXRD profile (black) and the simulated staggered AB stacking pattern (red) of TJNU-201. (Bottom) Unit cell of staggered AB stacking mode for TJNU-201.

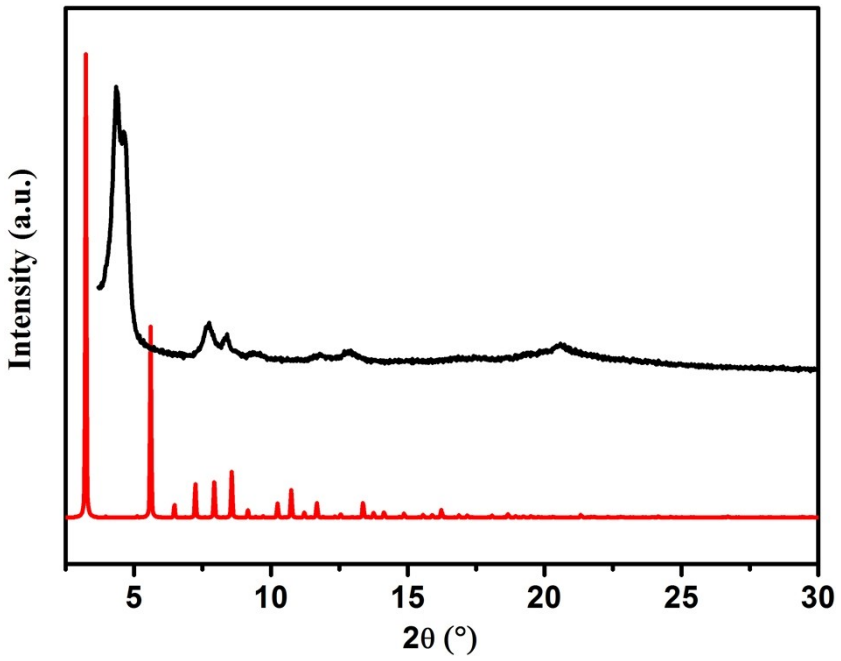


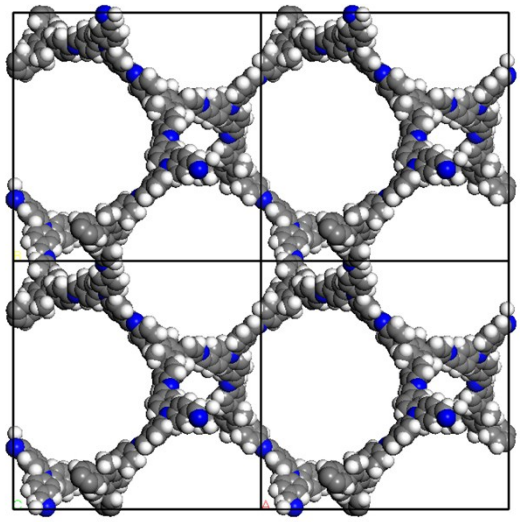

**Figure S16.** (Top) Experimental PXRD profile (black) and the simulated 3D structure with SrS topology (red) of TJNU-201. (Bottom) Unit cell of 3D structure with SrS topology for TJNU-201.

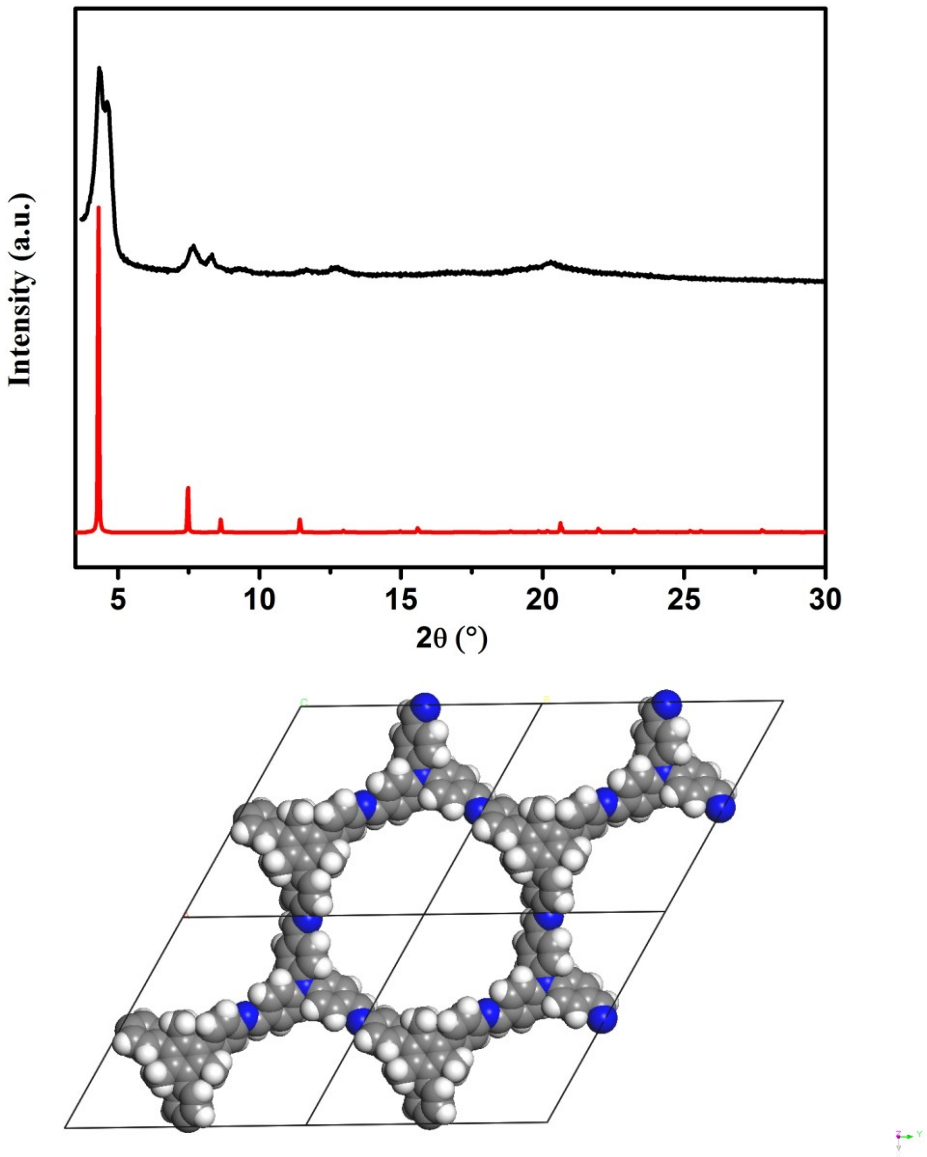


**Figure S17.** (Top) Experimental PXRD profile (black) and the simulated eclipsed AA stacking pattern (red) of TJNU-201. (Bottom) Unit cell of eclipsed AA stacking mode for TJNU-201.

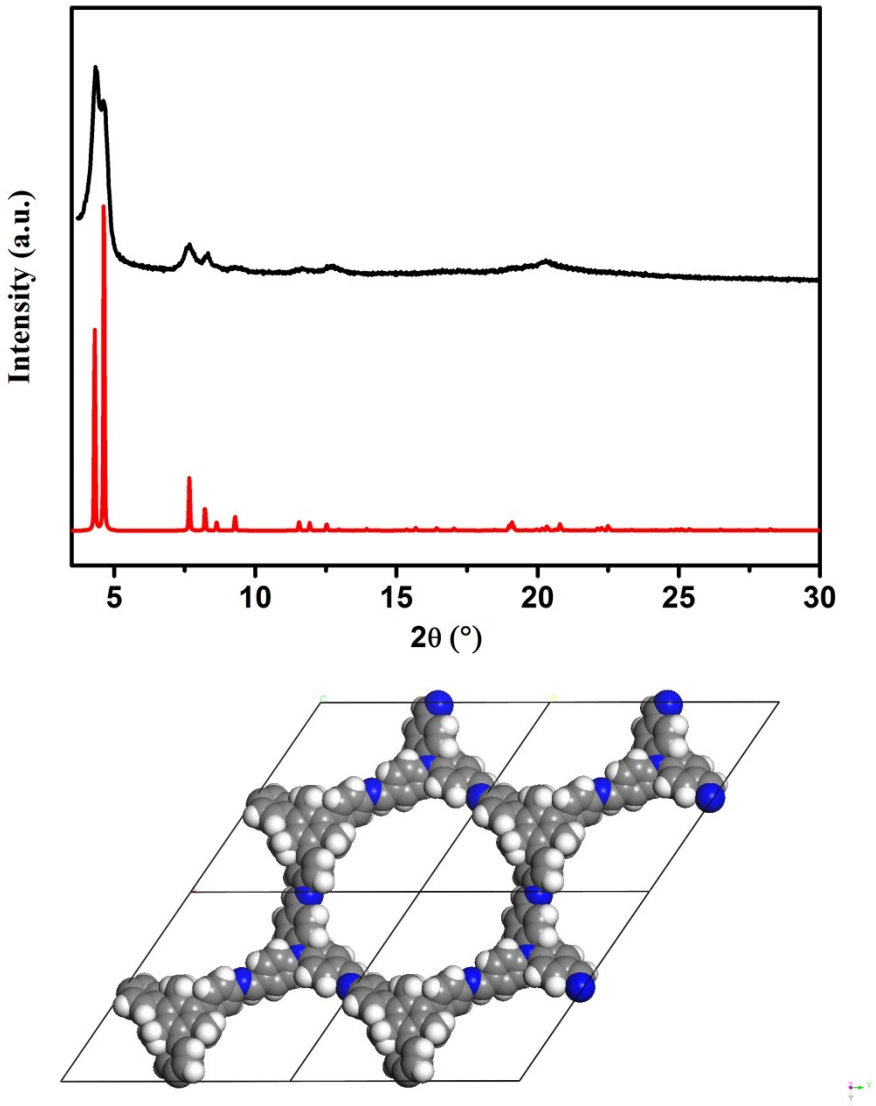


**Figure S18.** (Top) Experimental PXRD profile (black) and the simulated staircased stacking pattern (red) of TJNU-201. (Bottom) Unit cell of staircased stacking mode for TJNU-201.

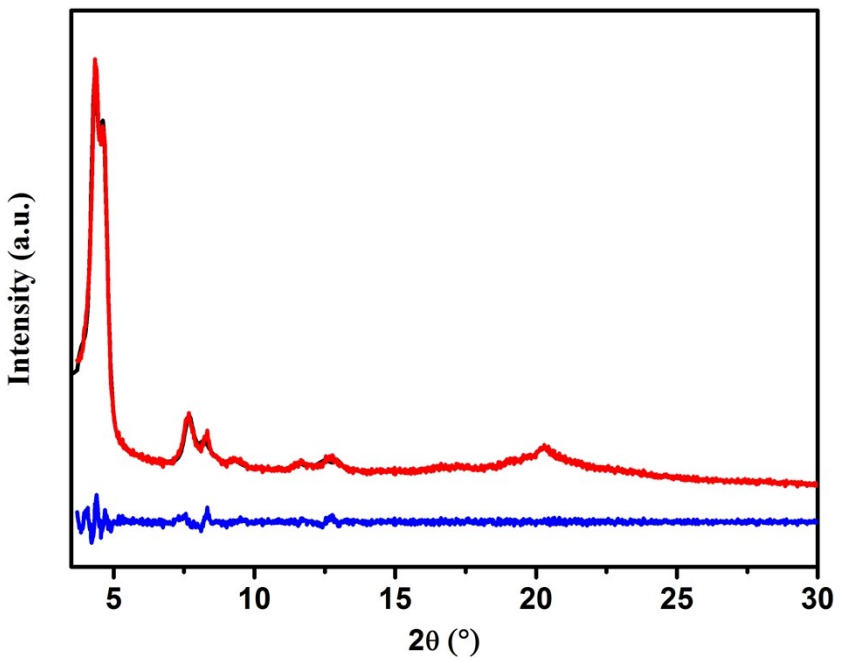


**Figure S19.** Experimental PXRD profile (red), Pawley refinement PXRD profile (black) of TJNU-201, and the differences between the experimental and refined PXRD patterns (blue).

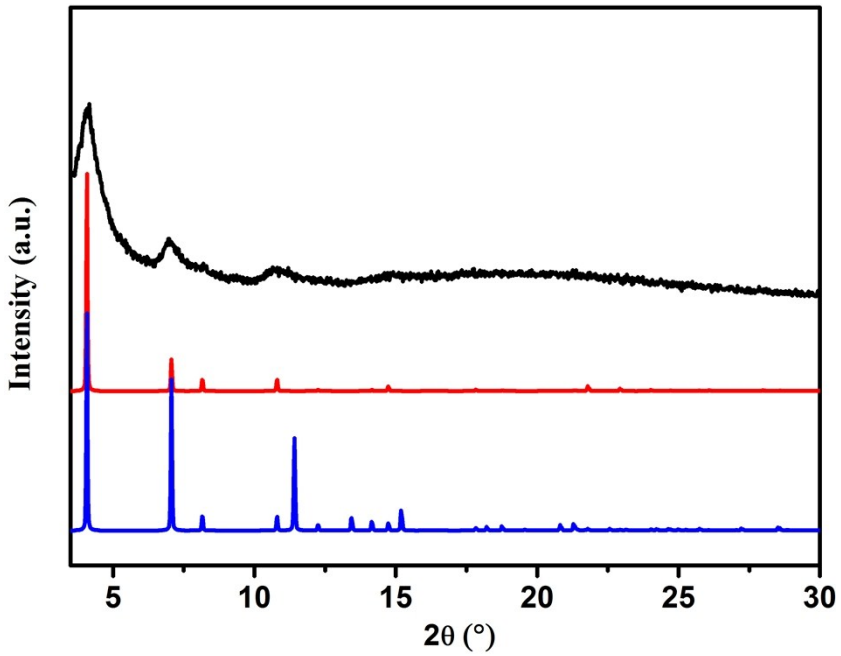


**Figure S20.** Experimental PXRD profile (black), the simulated eclipsed AA stacking pattern (blue), and staggered AB stacking pattern (red) of TJNU-202.

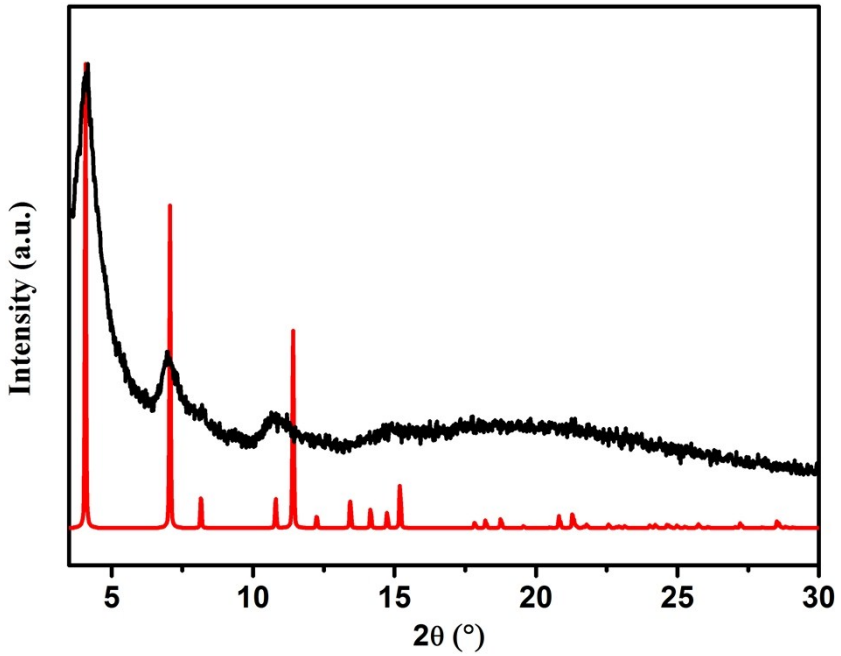


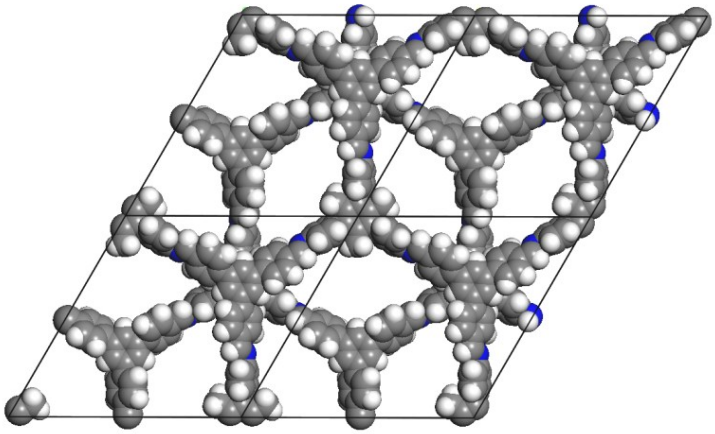

**Figure S21.** (Top) Experimental PXRD profile (black) and the simulated staggered AB stacking pattern (red) of TJNU-202. (Bottom) Unit cell of staggered AB stacking mode for TJNU-202.

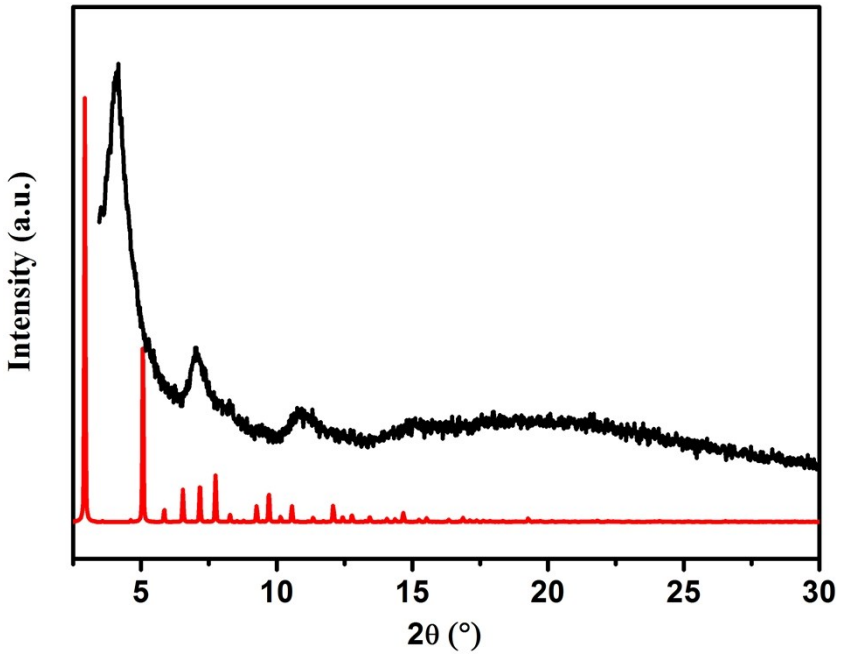


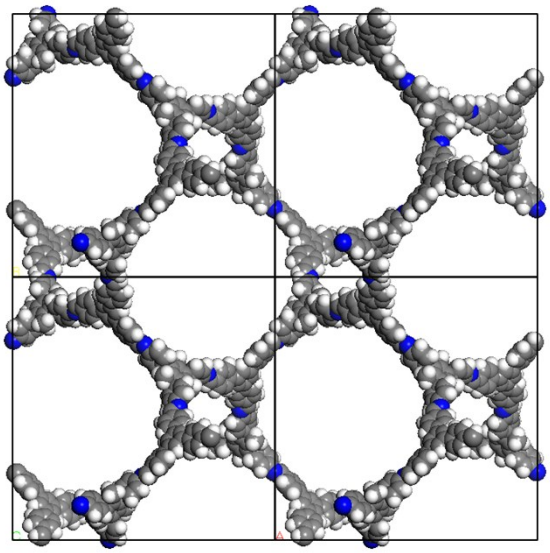

**Figure S22.** (Top) Experimental PXRD profile (black) and the simulated 3D structure with SrS topology (red) of TJNU-202. (Bottom) Unit cell of 3D structure with SrS topology for TJNU-202.

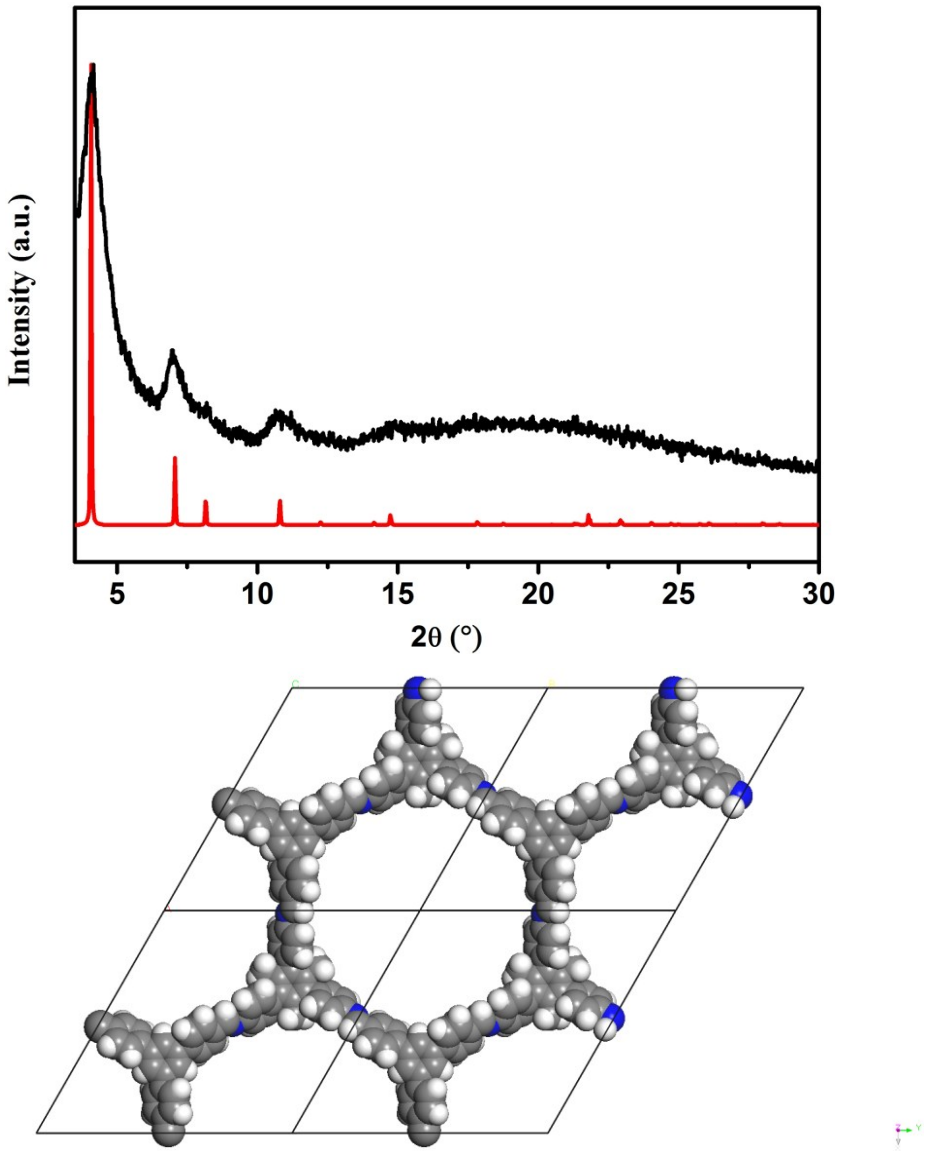


**Figure S23.** (Top) Experimental PXRD profile (black) and the simulated eclipsed AA stacking pattern (red) of TJNU-202. (Bottom) Unit cell of eclipsed AA stacking mode for TJNU-202.

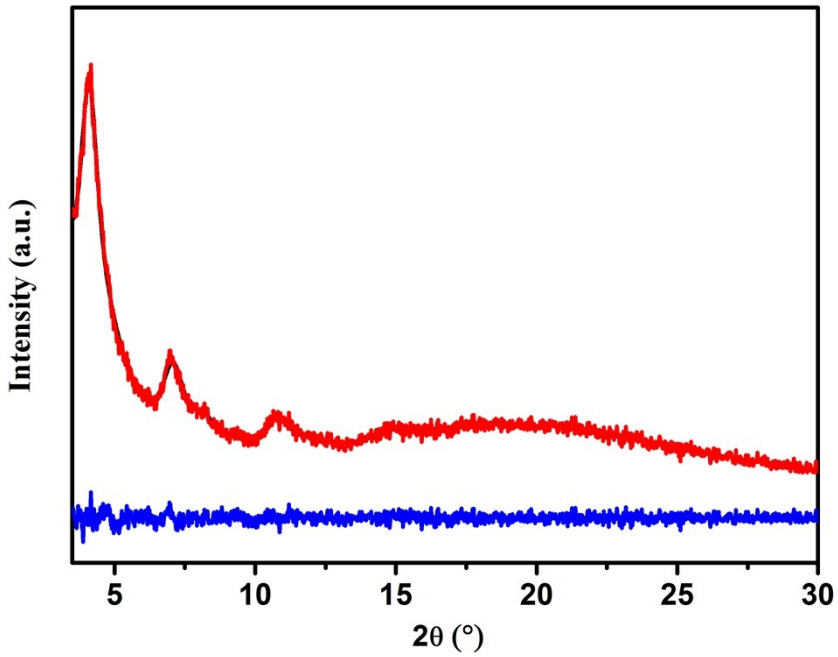


**Figure S24.** Experimental PXRD profile (red), Pawley refinement PXRD profile (black) of TJNU-202, and the differences between the experimental and refined PXRD patterns (blue).

**Table S1.** Fractional atomic coordinates for the unit cell of TJNU-201 calculated from the Materials Studio Modeling program.

| TJNU-201 space group: *P*1<br>*a* = *b* = 23.655 Å; *c* = 4.800 Å<br>*α* = *β*= 78°; *γ* = 120° | | | | |
|---|---|---|---|---|
| C1 | C | 0.73632 | 0.37389 | 0.75607 |
| C2 | C | 0.69558 | 0.40251 | 0.76792 |
| C3 | C | 0.72667 | 0.47594 | 0.80962 |
| C4 | C | 0.80910 | 0.41546 | 0.70001 |
| C5 | C | 0.85114 | 0.47062 | 0.86054 |
| C6 | C | 0.91827 | 0.50608 | 0.80773 |
| C7 | C | 0.94648 | 0.48538 | 0.60610 |
| C8 | C | 0.90544 | 0.42988 | 0.44666 |
| C9 | C | 0.83768 | 0.39749 | 0.48562 |
| N10 | N | 0.01641 | 0.52195 | 0.57385 |
| C11 | C | 0.05224 | 0.50711 | 0.41882 |
| C12 | C | 0.12418 | 0.54929 | 0.41306 |
| C13 | C | 0.15599 | 0.60871 | 0.55883 |
| C14 | C | 0.22410 | 0.64714 | 0.55340 |
| C15 | C | 0.26234 | 0.62716 | 0.40437 |
| C16 | C | 0.23003 | 0.56770 | 0.25820 |
| C17 | C | 0.16192 | 0.52942 | 0.26154 |
| H18 | H | 0.76334 | 0.50297 | 0.64495 |
| H19 | H | 0.74845 | 0.48904 | 1.01957 |
| H20 | H | 0.69271 | 0.49502 | 0.81527 |
| H21 | H | 0.83407 | 0.48480 | 1.04010 |
| H22 | H | 0.94909 | 0.54805 | 0.93613 |
| H23 | H | 0.92444 | 0.41222 | 0.28513 |
| H24 | H | 0.80733 | 0.35634 | 0.35378 |
| H25 | H | 0.03055 | 0.46277 | 0.29684 |
| H26 | H | 0.12835 | 0.62554 | 0.67787 |
| H27 | H | 0.24686 | 0.69260 | 0.66592 |
| H28 | H | 0.25749 | 0.55042 | 0.14319 |
| H29 | H | 0.13870 | 0.48388 | 0.14683 |
| C30 | C | 0.62611 | 0.36242 | 0.75607 |
| C31 | C | 0.59749 | 0.29307 | 0.76792 |
| C32 | C | 0.52406 | 0.25073 | 0.80962 |
| C33 | C | 0.58454 | 0.39364 | 0.70001 |
| C34 | C | 0.52938 | 0.38052 | 0.86054 |
| C35 | C | 0.49392 | 0.41219 | 0.80773 |
| C36 | C | 0.51462 | 0.46110 | 0.60610 |
| C37 | C | 0.57012 | 0.47556 | 0.44666 |
| C38 | C | 0.60251 | 0.44019 | 0.48562 |

| | | | | |
|---|---|---|---|---|
| N39 | N | 0.47805 | 0.49446 | 0.57385 |
| C40 | C | 0.49289 | 0.54513 | 0.41882 |
| C41 | C | 0.45071 | 0.57490 | 0.41306 |
| C42 | C | 0.39129 | 0.54727 | 0.55883 |
| C43 | C | 0.35286 | 0.57696 | 0.55340 |
| C44 | C | 0.37284 | 0.63518 | 0.40437 |
| C45 | C | 0.43230 | 0.66233 | 0.25820 |
| C46 | C | 0.47058 | 0.63250 | 0.26154 |
| H47 | H | 0.49703 | 0.26038 | 0.64495 |
| H48 | H | 0.51096 | 0.25940 | 1.01957 |
| H49 | H | 0.50498 | 0.19769 | 0.81527 |
| H50 | H | 0.51520 | 0.34927 | 1.04010 |
| H51 | H | 0.45195 | 0.40104 | 0.93613 |
| H52 | H | 0.58778 | 0.51222 | 0.28513 |
| H53 | H | 0.64366 | 0.45099 | 0.35378 |
| H54 | H | 0.53723 | 0.56778 | 0.29684 |
| H55 | H | 0.37446 | 0.50281 | 0.67787 |
| H56 | H | 0.30740 | 0.55426 | 0.66592 |
| H57 | H | 0.44958 | 0.70707 | 0.14319 |
| H58 | H | 0.51612 | 0.65481 | 0.14683 |
| C59 | C | 0.63758 | 0.26368 | 0.75607 |
| C60 | C | 0.70693 | 0.30442 | 0.76792 |
| C61 | C | 0.74927 | 0.27333 | 0.80962 |
| C62 | C | 0.60636 | 0.19090 | 0.70001 |
| C63 | C | 0.61948 | 0.14886 | 0.86054 |
| C64 | C | 0.58781 | 0.08173 | 0.80773 |
| C65 | C | 0.53890 | 0.05352 | 0.60610 |
| C66 | C | 0.52444 | 0.09456 | 0.44666 |
| C67 | C | 0.55981 | 0.16232 | 0.48562 |
| N68 | N | 0.50554 | 0.98359 | 0.57385 |
| C69 | C | 0.45487 | 0.94776 | 0.41882 |
| C70 | C | 0.42510 | 0.87582 | 0.41306 |
| C71 | C | 0.45273 | 0.84401 | 0.55883 |
| C72 | C | 0.42304 | 0.77590 | 0.55340 |
| C73 | C | 0.36482 | 0.73766 | 0.40437 |
| C74 | C | 0.33767 | 0.76997 | 0.25820 |
| C75 | C | 0.36750 | 0.83808 | 0.26154 |
| H76 | H | 0.73962 | 0.23666 | 0.64495 |
| H77 | H | 0.74060 | 0.25155 | 1.01957 |
| H78 | H | 0.80231 | 0.30729 | 0.81527 |
| H79 | H | 0.65073 | 0.16593 | 1.04010 |
| H80 | H | 0.59896 | 0.05091 | 0.93613 |
| H81 | H | 0.48778 | 0.07556 | 0.28513 |

| | | | | |
|---|---|---|---|---|
| H82 | H | 0.54901 | 0.19267 | 0.35378 |
| H83 | H | 0.43222 | 0.96945 | 0.29684 |
| H84 | H | 0.49719 | 0.87165 | 0.67787 |
| H85 | H | 0.44574 | 0.75314 | 0.66592 |
| H86 | H | 0.29293 | 0.74251 | 0.14319 |
| H87 | H | 0.34519 | 0.86130 | 0.14683 |
| N88 | N | 0.33333 | 0.66667 | 0.40289 |

**Table S2.** Fractional atomic coordinates for the unit cell of TJNU-202 calculated from the Materials Studio Modeling program.

| TJNU-202 space group: *P*3<br>$a = b = 25.022$ Å; $c = 4.150$ Å<br>$\alpha = \beta = 90°$; $\gamma = 120°$ | | | | |
|---|---|---|---|---|
| C1 | C | 0.36830 | 0.63817 | -0.09704 |
| C2 | C | 0.40401 | 0.60825 | -0.03686 |
| C3 | C | 0.39006 | 0.57164 | 0.19300 |
| C4 | C | 0.41909 | 0.53922 | 0.24338 |
| C5 | C | 0.46568 | 0.54573 | 0.07351 |
| C6 | C | 0.48083 | 0.58350 | -0.15078 |
| C7 | C | 0.44963 | 0.61345 | -0.20880 |
| N8 | N | 0.49870 | 0.51522 | 0.11857 |
| C9 | C | 0.49049 | 0.47742 | 0.31029 |
| C10 | C | 0.52812 | 0.44938 | 0.32667 |
| C11 | C | 0.51467 | 0.40435 | 0.51842 |
| C12 | C | 0.54882 | 0.37616 | 0.53289 |
| C13 | C | 0.59750 | 0.39311 | 0.35785 |
| C14 | C | 0.61148 | 0.43872 | 0.16834 |
| C15 | C | 0.57699 | 0.46647 | 0.15200 |
| C16 | C | 0.63296 | 0.36253 | 0.36858 |
| C17 | C | 0.69568 | 0.39584 | 0.36918 |
| C18 | C | 0.39675 | 0.70158 | -0.10685 |
| C19 | C | 0.60929 | 1.08675 | 0.65623 |
| H20 | H | 0.54804 | 1.19636 | 0.02869 |
| H21 | H | 0.49904 | 1.08743 | 0.00144 |
| H22 | H | 0.46456 | 0.73853 | -0.13017 |
| H23 | H | 0.65849 | 1.19609 | 0.68254 |
| H24 | H | 0.43317 | 0.78837 | 0.33014 |
| H25 | H | 0.48983 | 0.89491 | 0.41739 |
| H26 | H | 0.41154 | 0.92755 | -0.28610 |
| H27 | H | 0.36091 | 0.82121 | -0.39294 |
| H28 | H | 0.53513 | 0.99068 | 0.45881 |
| H29 | H | 0.72611 | 1.28185 | 0.36632 |
| H30 | H | 0.27104 | 0.75707 | 0.04221 |
| H31 | H | 0.21264 | 0.69540 | -0.13889 |
| H32 | H | 0.27113 | 0.75033 | -0.32415 |

## S9. Porosity and Specific Surface Area Analysis

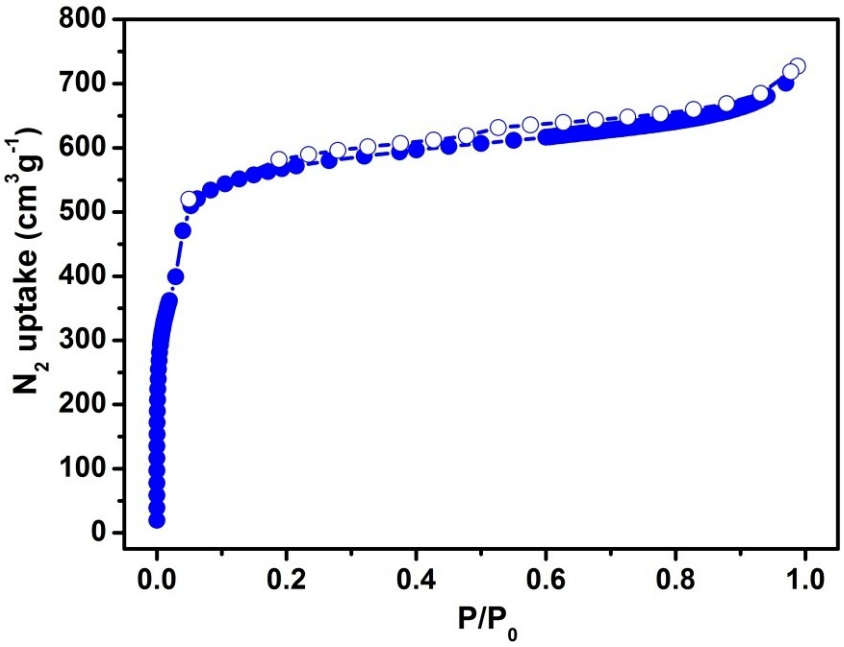


**Figure S25.** $N_2$ adsorption isotherm of TJNU-201 at 77 K.

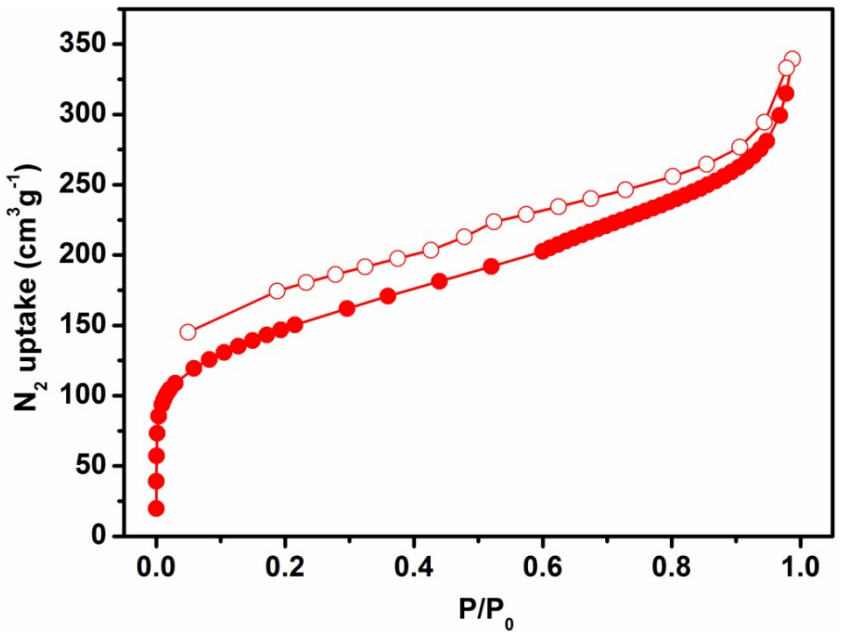


**Figure S26.** $N_2$ adsorption isotherm of TJNU-202 at 77 K.

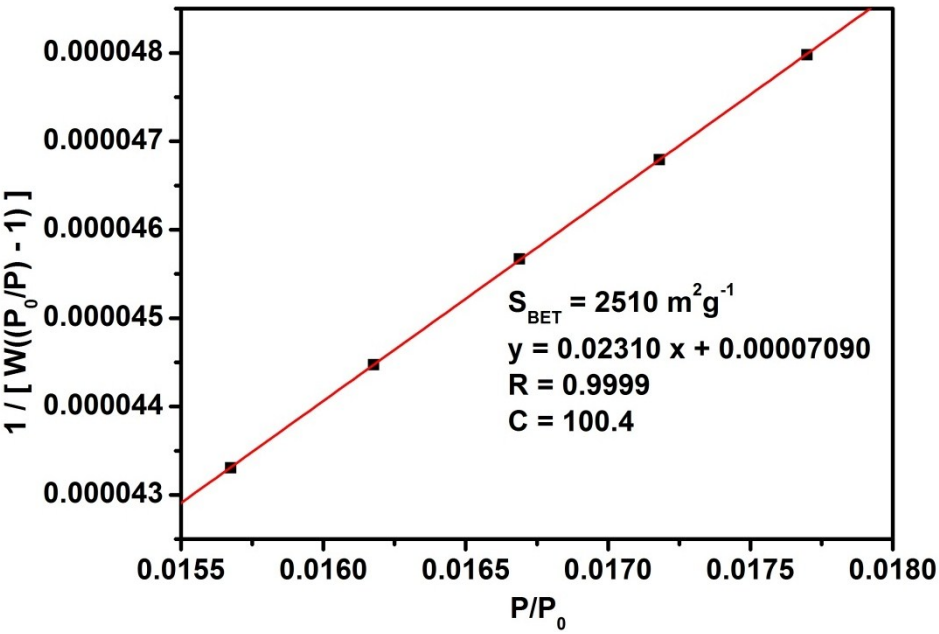


**Figure S27.** BET plot of TJNU-201 calculated from $N_2$ adsorption isotherm at 77 K, with C value of 100.4.

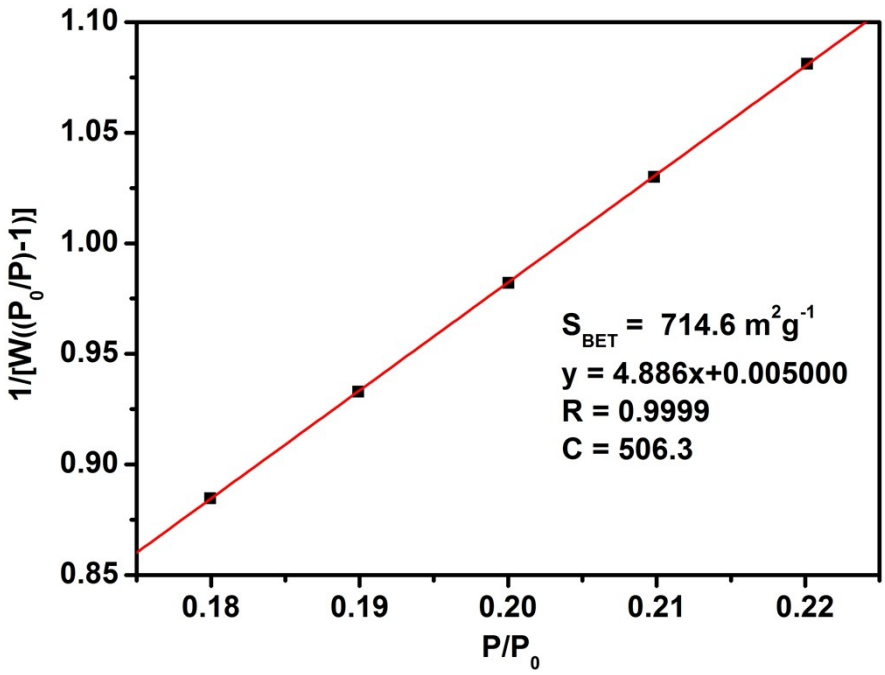


**Figure S28.** BET plot of TJNU-202 calculated from $N_2$ adsorption isotherm at 77 K, with C value of 506.3.

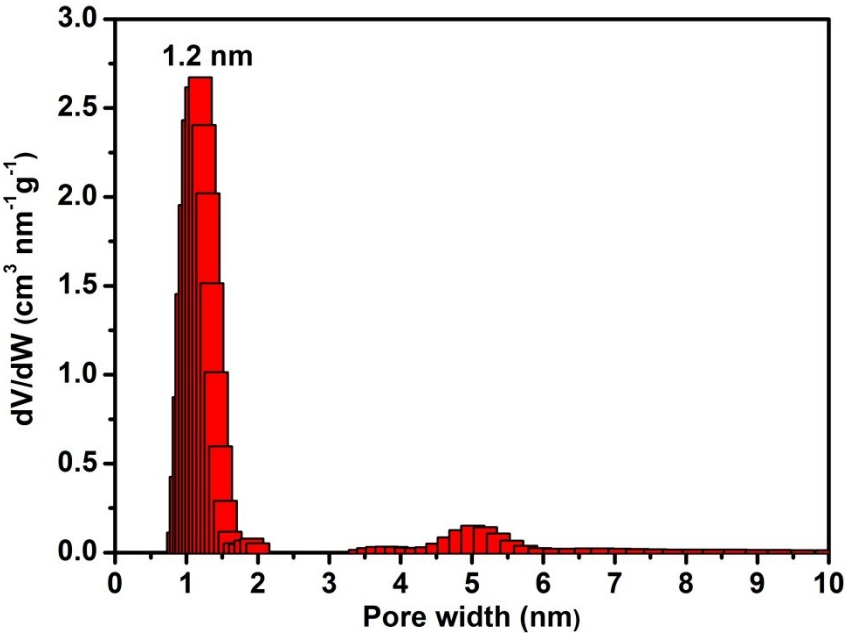


**Figure S29.** Pore size distribution of TJNU-201.

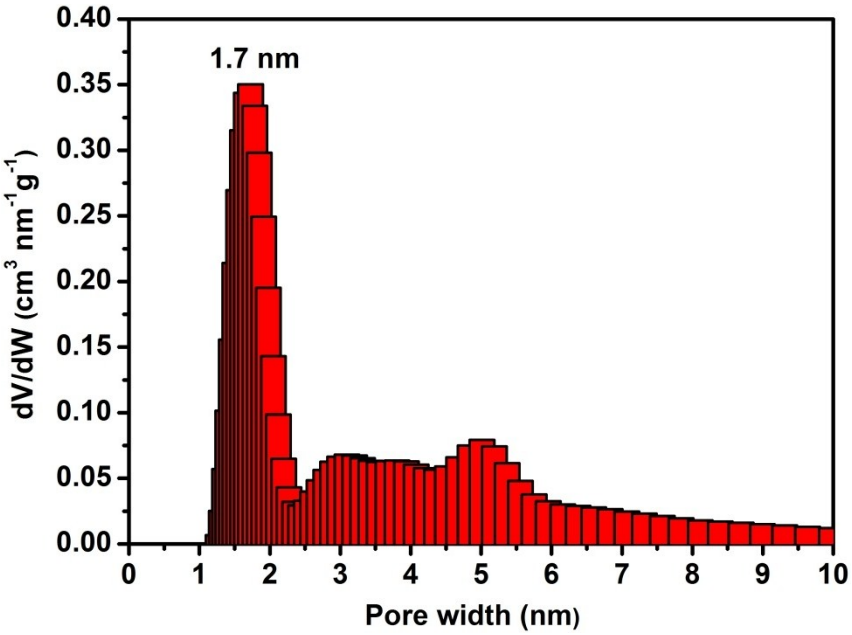


**Figure S30.** Pore size distribution of TJNU-202.

## S10. Iodine Vapor Uptake and Release Experiments

**General procedures for volatile iodine vapor uptake and release (three parallel tests were performed for all experiments, and the final values were shown as average values):**

**Iodine vapor capture:** The activated TJNU-201 (or TJNU-202) (20.0 mg) was placed in a vial (5 mL), and then the vial was exposed in a sealed container (20 mL) containing iodine (0.8 g). Next, the sealed container was heated at 350 K for 96 hours. After cooling to room temperature, the iodine-captured samples were taken out of the vial, collected and weighed.

**Iodine release:** The release process of iodine from $I_2$@TJNU-201 (or $I_2$@TJNU-202) was performed in methanol at room temperature and monitored by using UV/vis spectroscopy. $I_2$@TJNU-201 (or $I_2$@TJNU-202) (0.10 mg) was added to methanol (3 mL), and the content of iodine in methanol at different time was determined by UV/vis spectroscopy.

**Recycling of the COF samples:** The activated TJNU-201 (or TJNU-202) (20.0 mg) was placed in a vial (5 mL), and then the vial was exposed in a sealed container (20 mL) containing iodine (0.8 g). Next, the sealed container was heated at 350 K for 96 hours. After cooling to room temperature, the iodine-captured samples were taken out of the vial, collected and weighed. After iodine-captured COF sample was heated at 398 K for 24 h, the cooled sample was reused for the next cycle experiment.

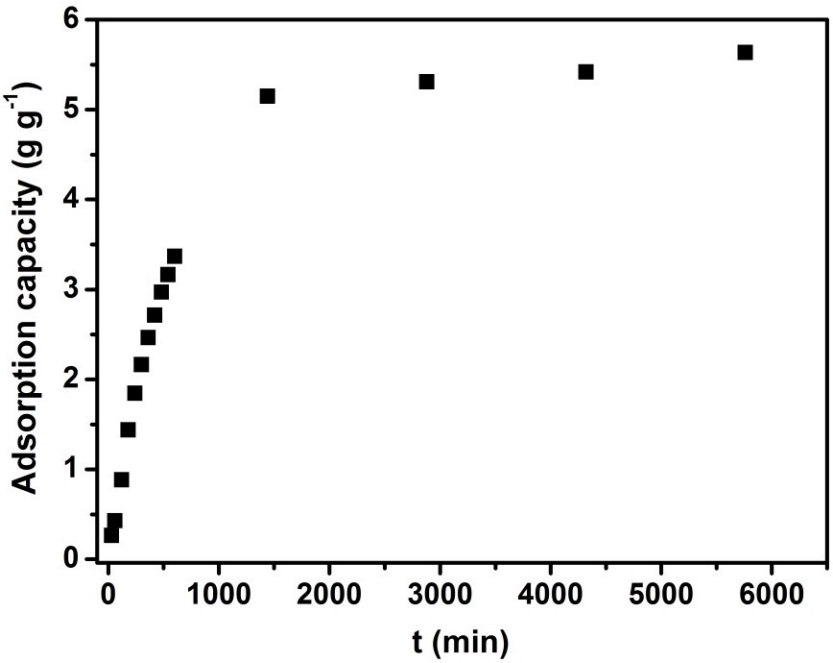


**Figure S31.** Gravimetric iodine uptake of TJNU-201 as a function of time at 350 K and ambient pressure.

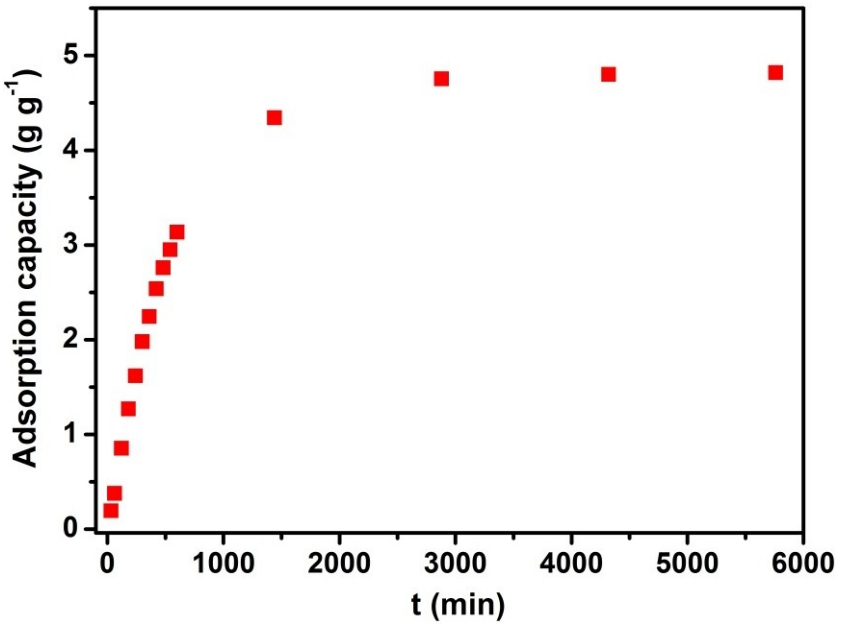


**Figure S32.** Gravimetric iodine uptake of TJNU-202 as a function of time at 350 K and ambient pressure.

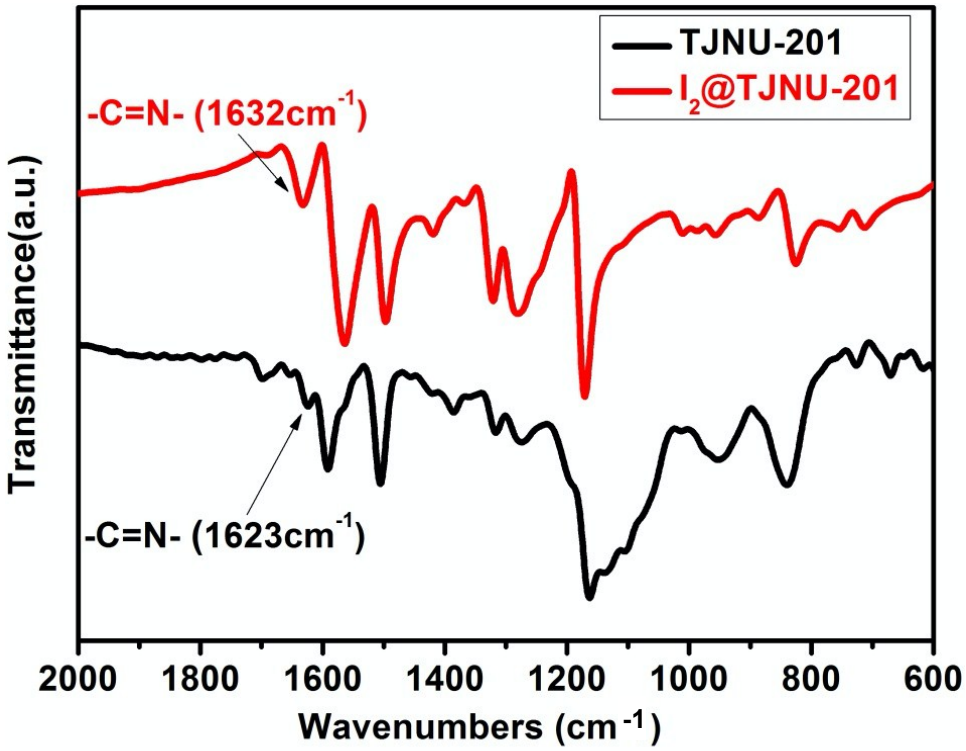


**Figure S33.** FT-IR spectra of TJNU-201 and $I_2$@TJNU-201.

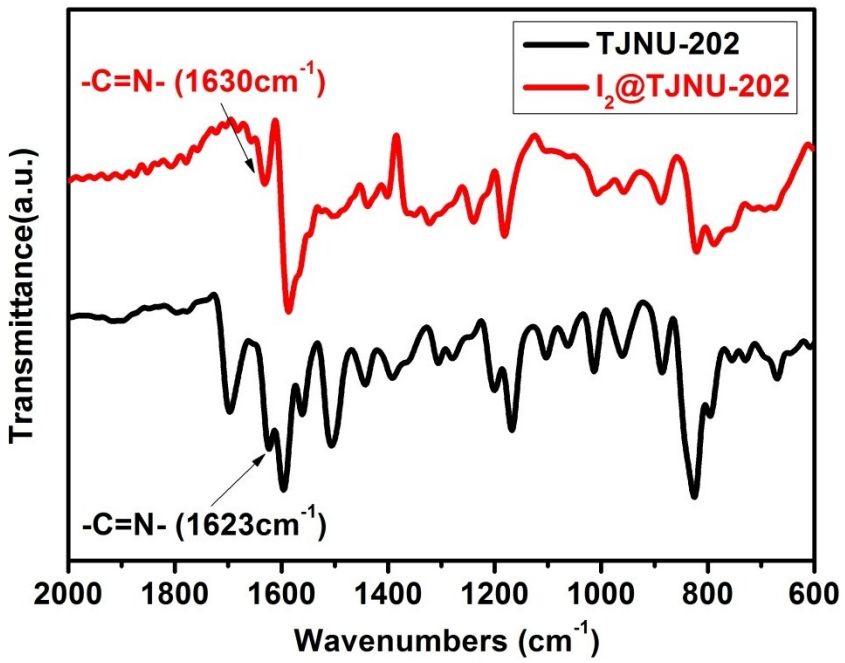


**Figure S34.** FT-IR spectra of TJNU-202 and $I_2$@TJNU-202.

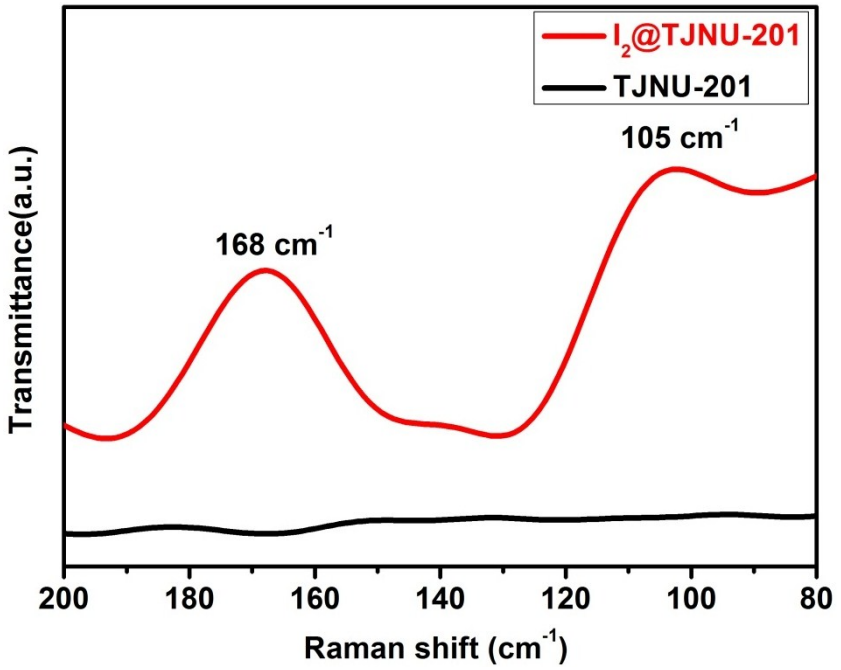


**Figure S35.** Raman spectra of TJNU-201 and $I_2$@TJNU-201.

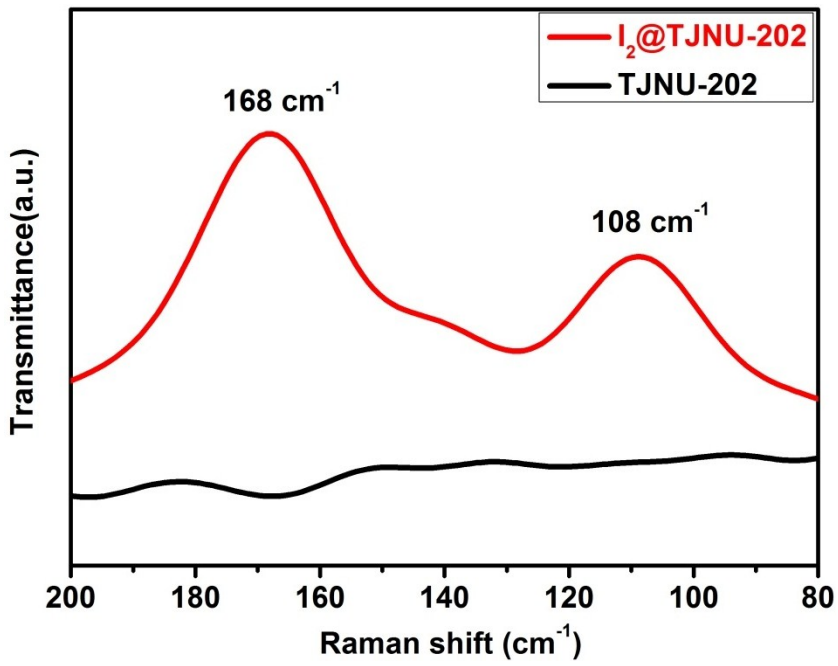


**Figure S36.** Raman spectra of TJNU-202 and $I_2$@TJNU-202.

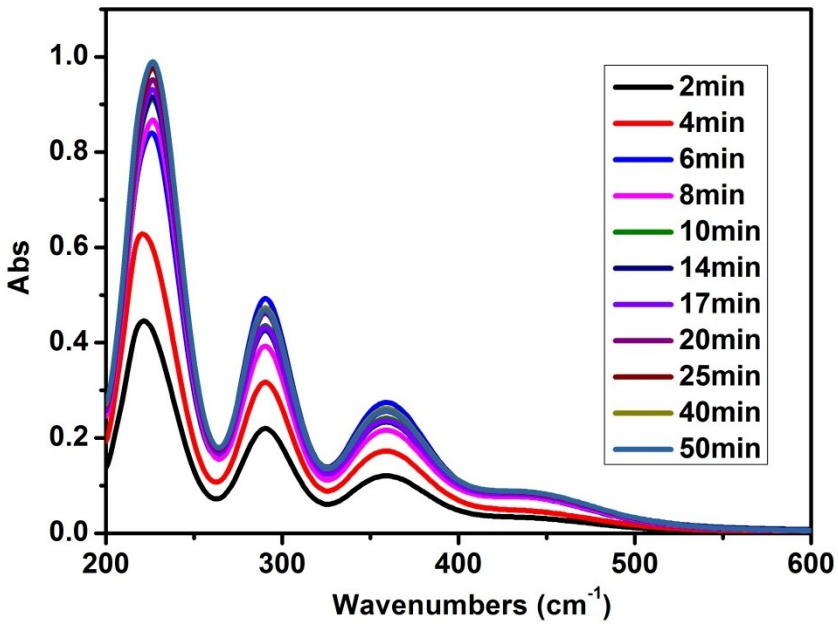


**Figure S37.** Release of iodine from $I_2$@TJNU-201 in the first 50 min monitored by UV/vis absorption spectra.

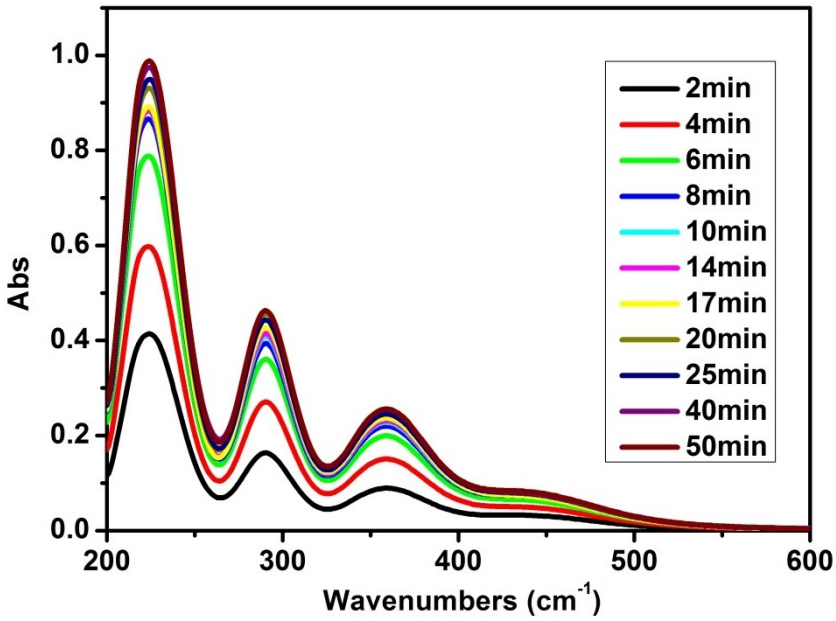


**Figure S38.** Release of iodine from $I_2$@TJNU-202 in the first 50 min monitored by UV/vis absorption spectra.

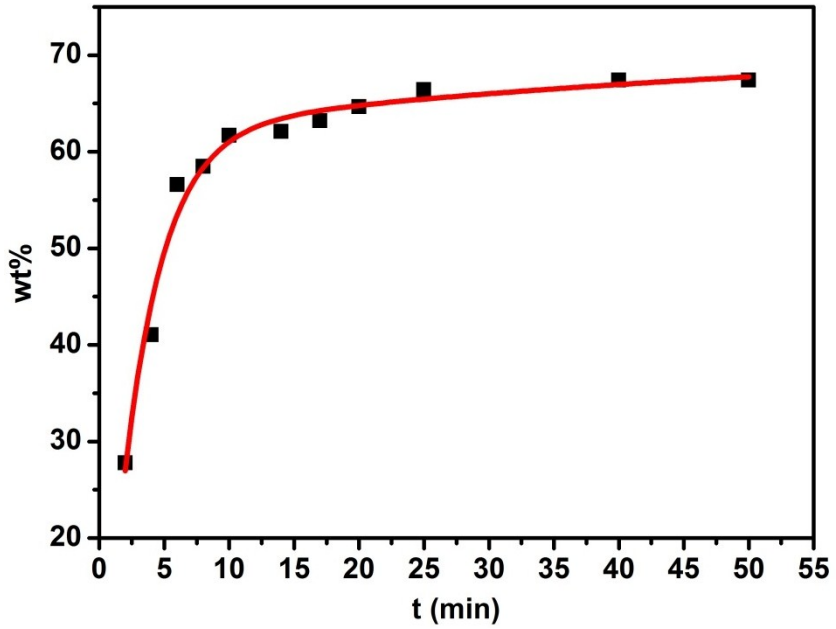


**Figure S39.** Release of iodine from $I_2$@TJNU-201 into methanol.

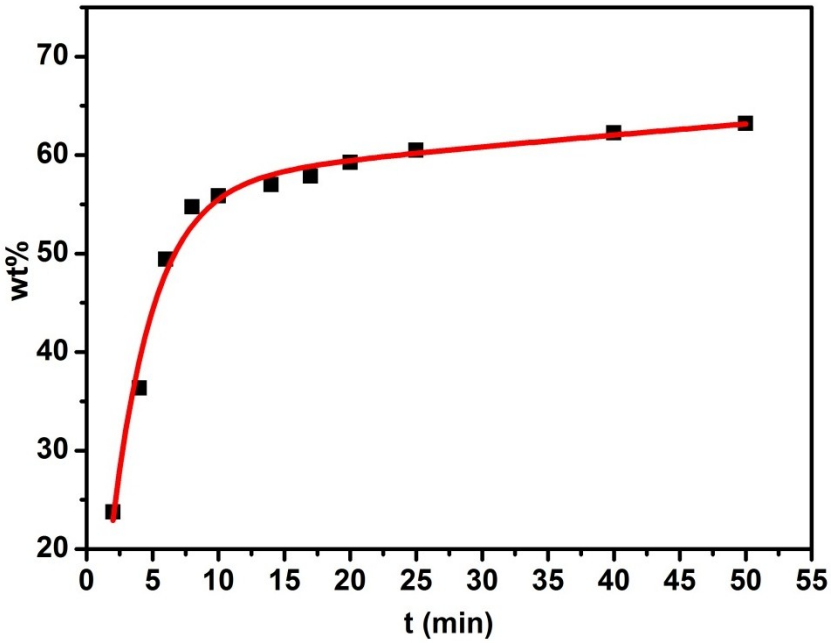


**Figure S40.** Release of iodine from $I_2$@TJNU-202 into methanol.

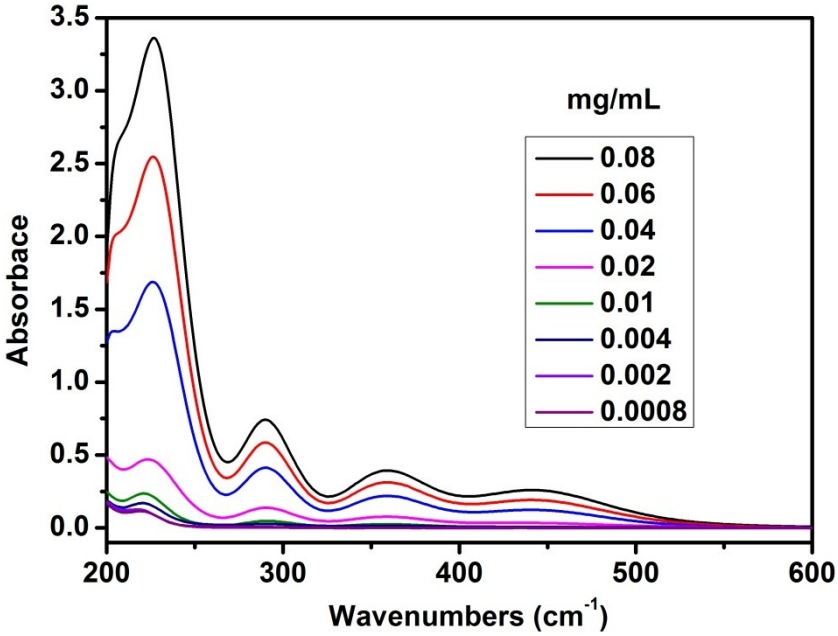


**Figure S41.** Calibration plot of standard iodine in methanol solution by UV/vis spectra.

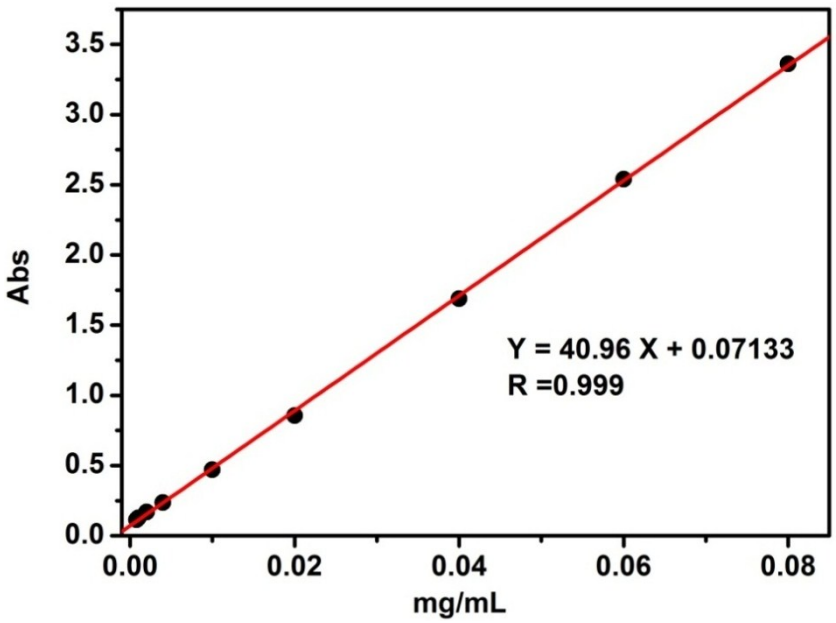


**Figure S42.** Fitting of absorbance value *vs* concentration of iodine. The good linearity satisfies Lambert-Beer Law.

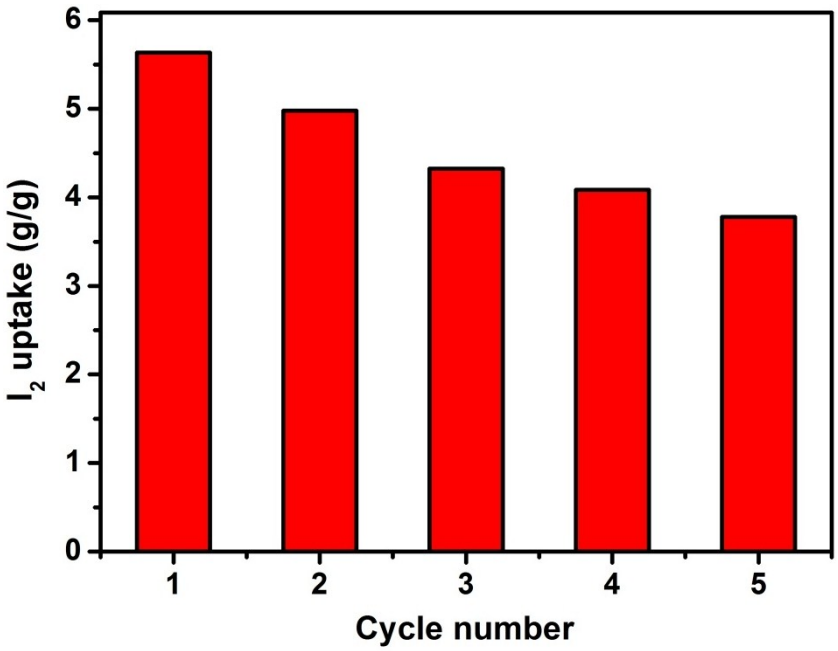


**Figure S43.** Recycling of TJNU-201 for iodine vapor capture.

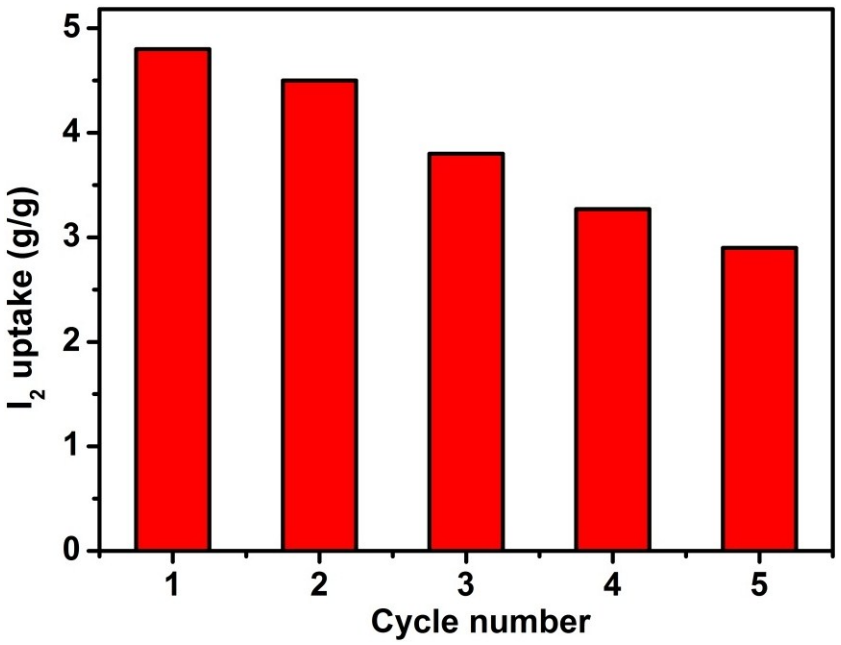


**Figure S44.** Recycling of TJNU-202 for iodine vapor capture.

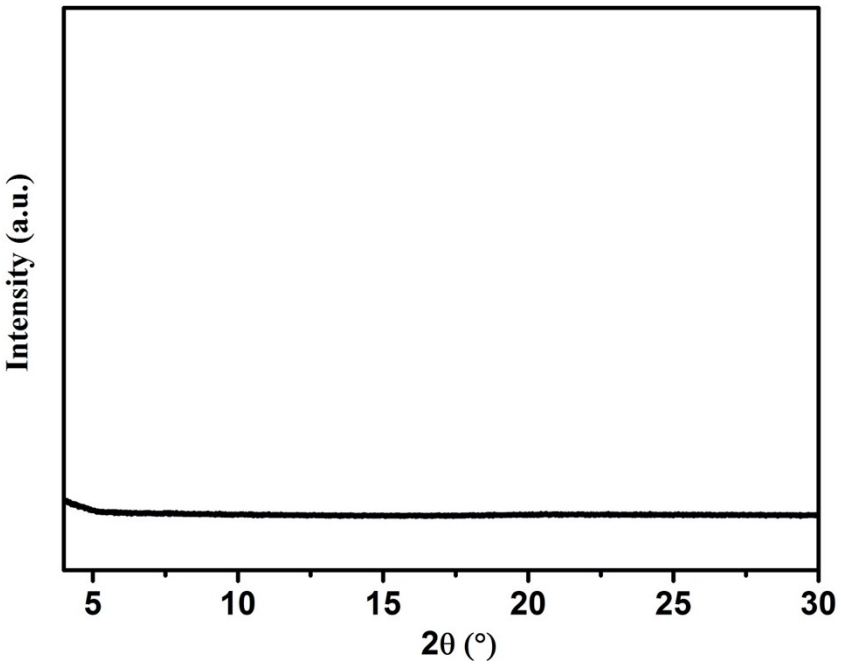


**Figure S45**. PXRD pattern of recycled TJNU-201 after five runs of iodine vapor capture.

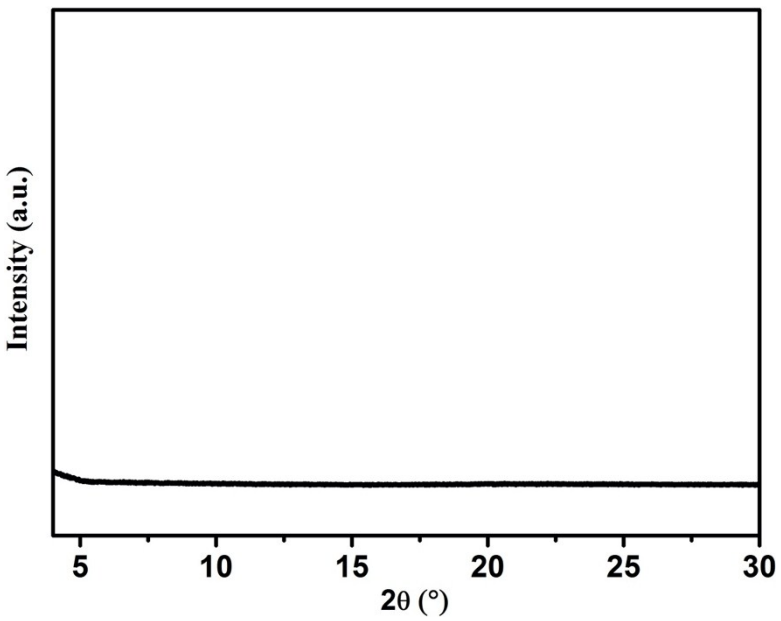


**Figure S46.** PXRD pattern of recycled TJNU-202 after five runs of iodine vapor capture.

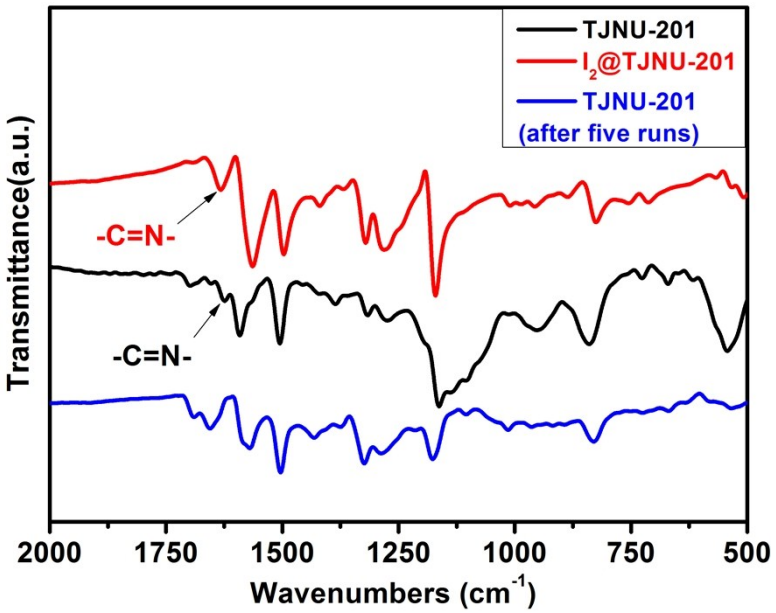


**Figure S47.** FT-IR spectra of recycled TJNU-201 after five runs of iodine vapor capture, indicating that the imine bond was completely broken.

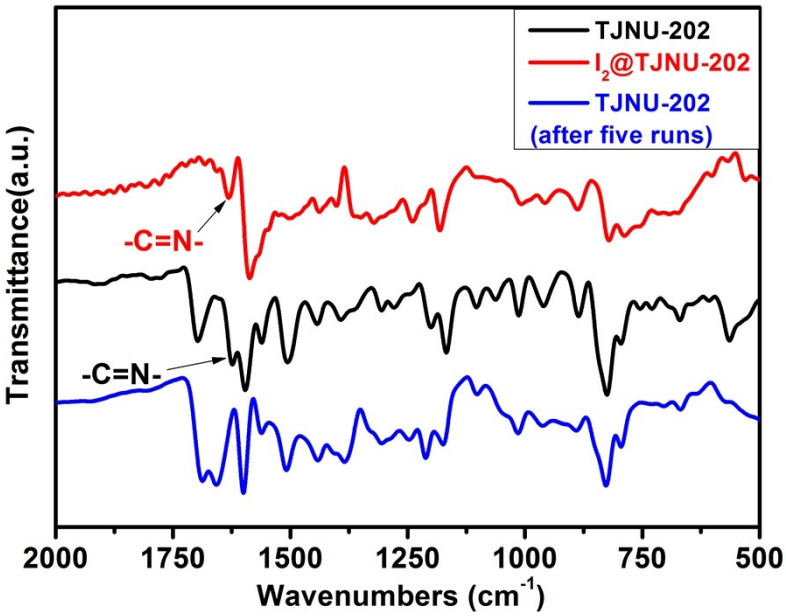


**Figure S48.** FT-IR spectra of recycled TJNU-202 after five runs of iodine vapor capture, indicating that the imine bond was completely broken.

**Table S3**. Iodine adsorption capacities in selected POPs, MOFs and COFs materials.

| Adsorbents | Temperature (°C) | Pressure | $S_{BET}$ ($m^2/g$) | Iodine capacity (g/g) | Ref. |
|---|---|---|---|---|---|
| TPB-DMTP COF | 75 | 1 bar | 1927 | 6.260 | S2 |
| TJNU-201 | 77 | 1 bar | 2510 | 5.625 | This work |
| TPT-BD COF | 75 | 1 bar | 109 | 5.430 | S3 |
| TTPPA | 77 | 1 bar | 512 | 4.900 | S4 |
| TJNU-202 | 77 | 1 bar | 714 | 4.820 | This work |
| SIOC-COF-7 | 75 | 1 bar | 618 | 4.810 | S5 |
| CalPOF-1 | 75 | 1 bar | 303 | 4.770 | S6 |
| ETTA-TPA | 75 | 1 bar | 1822 | 4.700 | S2 |
| COF-DL229 | 75 | 1 bar | 1762 | 4.680 | S7 |
| TTPB | 75 | 1 bar | 222 | 4.430 | S8 |
| NDB-H | 75 | 1 bar | 117 | 4.430 | S9 |
| NDB-S | 75 | 1 bar | 56 | 4.250 | S9 |
| Meso-COF-3 | 75 | 1 bar | 982 | 4.000 | S10 |
| POP-2 | 80 | 1 bar | 41 | 3.820 | S11 |
| POP-1 | 80 | 1 bar | 12 | 3.570 | S11 |
| HCMP-2, -3 | 85 | 1 bar | 153, 82 | 3.160, 3.360 | S12 |
| BDP-CPP-1, -2 | 75 | 1 bar | 635, 235 | 2.830, 2.230 | S13 |
| PAF-24 | 75 | 1 bar | 136 | 2.760 | S14 |
| PAF-23 | 75 | 1 bar | --- | 2.710 | S14 |
| PAF-25 | 75 | 1 bar | --- | 2.600 | S14 |
| Azo-Trip | 77 | 1 bar | 510 | 2.330 | S15 |
| CMPN-2, -3 | 70 | 1 bar | 339, 1368 | 1.100, 2.080 | S16 |
| NiP-CMP | 77 | 1 bar | 2630 | 2.020 | S17 |
| $N_3$-COF | 75 | 1 bar | 1240 | 1.950 | S18 |
| PAF-1 | 25 | 40 pa | 5600 | 1.860 | S19 |
| HKUST-1 MOF | 75 | 1 bar | 1850 | 1.750 | S20 |
| ZIF-8 MOF | 77 | 1 bar | 1630 | 1.250 | S21 |
| UiO-66-PYDC MOF | 25 | 1 bar | 1030 | 1.250 (solution) | S22 |
| Activated carbon | 75 | 1 bar | --- | 0.300 | S23 |
| Ag@Zeolite Mordenites | 95 | 1 bar | --- | 0.275 | S24 |
| Ag@Mon-POF | 70 | 1 bar | 690 | 0.250 | S25 |

## S11. References


S1. Accelrys, Material Studio Release Notes, Release 4.4, Accelrys Software, San Diego 2008.

S2. P. Wang, Q. Xu, Z. Li, W. Jiang, Q. Jiang and D. Jiang, *Adv. Mater.*, 2018, **30**, 1801991.

S3. X. Guo, Y. Tian, M. Zhang, Y. Li, R. Wen, X. Li, X. Li, Y. Xue, L. Ma, C Xia and S. Li, *Chem. Mater.*, 2018, **30**, 2299-2308.

S4. T. Geng, S. Ye, Z. Z. Zhu and W. Hang, *J. Mater. Chem. A.*, 2018, **6**, 2808-2816.

S5. Z. J. Yin, S. Q. Xu, T. G. Zhan, Q. Y. Qi, Z. Q. Wu and X. Zhao, *Chem. Commun.*, 2017, **53**, 7266-7269.

S6. K. Su, W. Wang, B.-B. Li, and D. Yuan, *ACS Sustain. Chem. Eng.*, 2018, **6**, 17402-17409.

S7. C. Wang, Y. Wang, R. Ge, X. Song, X. Xing, Q. Jiang, H. Lu, C. Hao, X. Guo Y. Gao and D. Jiang, *Chem. Eur. J.*, 2018, **24**, 585-589.

S8. T. Geng, Z. Zhu, W. Zhang and Y. Wang, *J. Mater. Chem. A.*, 2017, **5**, 7612-7617.

S9. Z. Guo, P. Sun, X. Zhang, J. Lin, T. Shi, S. Liu, A. Sun and Z. Li, *Chem. Asian J.*, 2018, **13**, 2046-2053.

S10. S. An, X. Zhu, Y. He, L. Yang, H. Wang, S. Jin, J. Hu and H. Liu, *Ind. Eng. Chem. Res.*, 2019, **58**, 10495-10502.

S11. X. Qian, B. Wang, Z. Q. Zhu, H. X. Sun, F. Ren, P. Mu, C. Ma, W. D. Liang and A. Li, *J. Hazard. Mater.*, 2017, **338**, 224-232.

S12. Y. Liao, J. Weber, B. M. Mills, Z. Ren and C. F. Faul, *Macromolecules*, 2016, **49**, 6322-6333.

S13. Y. Zhu, Y.-J. Ji, D.-G. Wang, Y. Zhang, H. Tang, X.-R. Jia, M. Song, G. Yu and G.-C. Kuang, *J. Mater. Chem. A*, 2017, **5**, 6622-6629.

S14. Z. Yan, Y. Yuan, Y. Tian, D. Zhang and G. Zhu, *Angew. Chem., Int. Ed.*, 2015, **54**, 12733-12737.

S15. Q. Q. Dang, X. M. Wang, Y. F. Zhan and X. M. Zhang, *Polym. Chem.*, 2016, **7**, 643-647.

S16. Y. Chen, H. Sun, R. Yang, T. Wang, C. Pei, Z. Xiang, Z. Zhu, W. Liang, A. Li and W. Deng, *J. Mater. Chem. A*, 2015, **3**, 87-91.

S17. A. Sigen, Y. Zhang, Z. Li, H. Xia, M. Xue, X. Liu and Y. Mu, *Chem. Commun.*, 2014, **50**, 8495-8498.

S18. V. S. Vyas, F. Haase, L. Stegbauer, G. Savasci, F. Podjaski, C. Ochsenfeld and B. V. Lotsch, *Nat. Commun.*, 2015, **6**, 8508.

S19. C. Pei, T. Ben, S. Xu and S. Qiu, *J. Mater. Chem. A*, 2014, **2**, 7179-7187.

S20. D. F. Sava, K. W. Chapman, M. A. Rodriguez, J. A. Greathouse, P. S. Crozier, H. Y. Zhao, P. J. Chupas and T. M. Nenoff, *Chem. Mater.*, 2013, **25**, 2591-2596.

S21. D. F. Sava, M. A. Rodriguez, K. W. Chapman, P. J. Chupas, J. A. Greathouse, P. S. Crozier and T. M. Nenoff, *J. Am. Chem. Soc.*, 2011, **133**, 12398-12401.

S22. Z. Wang, Y. Huang, J. Yang, Y. Li, Q. Zhuang and J. Gu, *Dalton Trans.*, 2017, **46**, 7412-7420.

S23 H. Ma, J. J. Chen, L. Tan, J. H. Bu, Y. Zhu, B. Tan and C. Zhang, *ACS Macro. Lett*., 2016, **5**, 1039-1043

S24. K. W. Chapman, P. J. Chupas and T. M. Nenoff, *J. Am. Chem. Soc.*, 2010, **132**, 8897-8899.

S25. A. P. Katsoulidis, J. He and M. G. Kanatzidis, *Chem. Mater*., 2012, **24**, 1937-1943.